ARTICLE IN PRESS

Geochimica et Cosmochimica Acta xxx (xxxx) xxx

ELSEVIER

Contents lists available at ScienceDirect

Geochimica et Cosmochimica Acta

journal homepage: www.elsevier.com/locate/gca



The non-carbonaceous nature of Earth's late-stage accretion

K.R. Bermingham ^{a,b,*}, H.A. Tornabene ^{a,b}, R.J. Walker ^b, L.V. Godfrey ^a, B.S. Meyer ^c, P. Piccoli ^b, S.J. Mojzsis ^{d,e,f,g}

- ^a Department of Earth and Planetary Sciences, Rutgers University, Piscataway, NJ 08854 USA
- ^b Department of Geology, University of Maryland, College Park, MD 20742 USA
- ^c Department of Physics and Astronomy, Clemson University, Clemson SC 29631 USA
- d HUN-REN, Research Centre for Astronomy and Earth Sciences (CSsFK), MTA Centre for Excellence, 1121 Budapest, Hungary
- ^e Department of Lithospheric Research, University of Vienna, UZA 2, Josef-Holaubek-Platz 2, 1090 Vienna, Austria
- f Department of Geosciences, Centre for Planetary Habitability (PHAB), University of Oslo, Postboks 1028 Blindern 0316 Oslo, Norway
- g Institute for Earth Sciences, Friedrich-Schiller University, Burgweg 11, 07749 Jena, Germany

ARTICLE INFO

Keywords: Mo isotopes NC-CC genetics Late-stage accretion Volatile/water delivery

ABSTRACT

Constraining the origin of Earth's building blocks requires knowledge of the chemical and isotopic characteristics of the source region(s) where these materials accreted. The siderophile elements Mo and Ru are well suited to investigating the mass-independent nucleosynthetic (i.e., "genetic") signatures of material that contributed to the latter stages of Earth's formation. Studies contrasting the Mo and Ru isotopic compositions of the bulk silicate Earth (BSE) to genetic signatures of meteorites, however, have reported conflicting estimates of the proportions of the non-carbonaceous type or NC (presumptive inner Solar System origin) and carbonaceous chondrite type or CC (presumptive outer Solar System origin) materials delivered to Earth during late-stage accretion (likely including the Moon-forming event and onwards). The present study reports new mass-independent isotopic data for Mo, which are presumed to reflect the composition of the BSE. A comparison of the new estimate for the BSE composition with new data for a select suite of NC iron meteorites is used to constrain the genetic characteristics of materials accreted to Earth during late-stage accretion. Results indicate that the final 10 to 20 wt% of Earth's accretion was dominated by NC materials that were likely sourced from the inner Solar System, although the addition of minor proportions of CC materials, as has been suggested to occur during accretion of the final 0.5 to 1 wt% of Earth's mass, remains possible. If this interpretation is correct, it brings estimates of the genetic signatures of Mo and Ru during the final 10 to 20 wt% of Earth accretion into concordance.

1. Introduction

Earth formed from the sequential accretion of planetesimals (i.e., "building blocks") that were likely sourced from different heliocentric distances (Kokubo and Ida, 1998). Understanding the planet's formation, therefore, requires knowledge of where in the early Solar System Earth's dominant building blocks accreted. Mass-independent nucleosynthetic (i.e., "genetic") isotope variations are well documented in bulk meteorites. Genetic variations among meteorites are the result of an imperfect mixing of presolar carriers in the protoplanetary disk (e.g., Dauphas et al., 2002; Trinquier et al., 2007). At the Solar System scale, genetic isotope compositions of elements such as Ti and Cr in bulk meteorites have been used to distinguish the so-called non-carbonaceous (NC) from carbonaceous chondrite (CC) type parent bodies, which have

been proposed to reflect a parent body's formation in the inner or outer Solar System, respectively (Warren, 2011). The separation and subsequent isolation of the NC-CC reservoirs may have been modulated by the early formation of Jupiter, annular ring structures present in the protoplanetary disk, or migration of the snowline (Warren, 2011; Kruijer et al., 2017; Brasser and Mojzsis, 2020; Lichtenberg et al., 2021; Izidoro et al., 2021). Important here is the recognition that genetic isotope compositions are sensitive tracers that can be used to identify the origin of Earth's dominant building blocks throughout the accretion process (Dauphas, 2017).

For several reasons, the siderophile (iron-loving) elements Mo and Ru are particularly well suited to investigating the genetics of building blocks participating in the latter stages of Earth's formation. First, these elements are commonly used genetic tracers that discriminate among

E-mail address: katherine.bermingham@rutgers.edu (K.R. Bermingham).

https://doi.org/10.1016/j.gca.2024.11.005

Received 8 March 2024; Accepted 2 November 2024

Available online 5 November 2024

0016-7037/© 2024 The Authors. Published by Elsevier Ltd. This is an open access article under the CC BY-NC license (http://creativecommons.org/licenses/by-nc/4.0/).

 $^{^{\}ast}$ Corresponding author.

NC and CC origins of meteorites (e.g., Fischer-Gödde et al., 2015; Budde et al., 2016; Kruijer et al., 2017; Bermingham et al., 2018). Second, variations in the Mo and Ru isotopic compositions of most meteorites are correlated, a characteristic that was termed the "cosmic Mo-Ru isotope correlation" by Dauphas et al. (2004). The correlation was interpreted in that study to indicate that the genetic variations observed among different types of meteorites were likely caused by the heterogeneous distribution of the same type of s-process presolar carriers, possibly mainstream circumstellar SiC grains. This interpretation has been supported by higher-resolution datasets of a wider selection of major iron meteorite groups, which define a correlation within the NC group and between the NC group and most CC meteorites (Bermingham et al., 2018; Worsham et al., 2019; Hopp et al., 2020). Third, most of the Mo and Ru present in the bulk silicate Earth (BSE) was likely added during different periods of Earth's late stages of accretion. The dominant share of the moderately siderophile Mo was likely established in the BSE during the final 10 to 20 wt% of Earth's accretion, coincident and including a final giant impact event that led to the formation of the Moon and the end stages of core segregation (Dauphas et al., 2004; Dauphas, 2017; Jennings et al., 2021). Late-stage addition of Mo to the BSE is a consequence of the decrease in metal-silicate distribution coefficients as the planet grew and metal-silicate segregation occurred at increasingly higher pressures and temperatures. Thus, most of the Mo residing in the BSE was added as Earth approached its current mass (Dauphas, 2017). By contrast, the highly siderophile Ru in the BSE was likely predominantly added during the final 0.5 to 2 wt% of Earth's accretion following core formation by a process termed "late accretion" or "late veneer" (Kimura et al., 1974; Chou, 1978; Walker, 2009; Marchi et al., 2018; Brasser et al., 2018). The assumption that Ru in the BSE was primarily added by late accretion stems from the very high metal-silicate distribution coefficients, which likely prevented the substantial build-up of Ru in the BSE until core formation ceased. Therefore, the Mo and Ru isotopic compositions of the BSE may provide complementary genetic information about the NC or CC nature of Earth's late-stage building blocks and the dynamical history of the early Solar System.

Studies examining the Mo and Ru isotopic compositions of the BSE and their relations to the genetic signatures of meteorites have reported conflicting estimates of the fraction of NC and CC materials accreted to Earth during the latter stages of accretion. Using a BSE composition presumed to be that of laboratory standards, Dauphas et al. (2004) observed that the $\mu^{92}\text{Mo}$ and $\mu^{100}\text{Ru}$ isotopic estimates of the BSE plot at the most *s*-process-enriched end of the cosmic correlation, a composition that is now recognized as having NC genetics (Bermingham et al., 2018). The μ -notation refers to the deviation in parts per million in the isotopic composition of a sample relative to terrestrial laboratory standards. Dauphas et al. (2004) recognized an implication of the relative position of BSE to the cosmic correlation is that Earth's feeding zone did not substantially change during the latter stages of accretion. Bermingham and Walker (2017) and Bermingham et al. (2018) reported an estimate of the $\mu^{97} Mo$ and $\mu^{100} Ru$ isotopic composition of the BSE by averaging the isotopic compositions measured on a global distribution of modern terrestrial materials. These studies noted that both the μ^{97} Mo and μ^{100} Ru compositions estimated for the BSE are most similar to certain NC parent bodies, notably IAB main group iron meteorites. As in the Dauphas et al. (2004) study, Bermingham et al. (2018) inferred that the final 10 to 20 wt% of Earth's accretion, including materials added by the final 0.5 to 2 wt% of late accretion, was dominated by NC materials and that there was no major change in the genetic composition of accreted material during this period.

In contrast to findings of dominantly NC contributors to Earth's late-stage accretion, Budde et al. (2019) determined Mo isotopic compositions for several terrestrial materials and meteorites. That study reported that the isotopic composition of the BSE falls between parallel, linear correlations defined by data for NC– and CC-type meteorites when plotted on a $\mu^{94}\text{Mo}$ versus $\mu^{95}\text{Mo}$ diagram, which is commonly used to discern meteorite genetics. Based on this intermediate isotopic

composition of the BSE, that study concluded Earth accreted 46 \pm 15 % of CC material during the final 10 to 20 wt% of Earth's formation, possibly during the Moon-forming impact. The conclusion of Budde et al. (2019) was supported by follow-up studies (Archer et al., 2023; Budde et al., 2023). The studies of Dauphas et al. (2004) and Bermingham et al. (2018) did not have sufficient resolution for $\mu^{94}\text{Mo}$ and $\mu^{95}\text{Mo}$ measurements of the BSE to estimate NC vs. CC contributions to the BSE using these isotopes.

Ruthenium isotopes present additional complexity with respect to Earth's genetics. Studies of the mass-independent isotopic composition of Ru in the modern BSE have reported that it is characterized by Ru that is similar to that present in NC enstatite chondrites and main group IAB iron meteorites (Fischer-Gödde and Kleine, 2017; Bermingham and Walker, 2017; Bermingham et al., 2018). The BSE Ru isotopic estimate has among the most s-process-rich Ru compositions of known bulk planetary materials. Fischer-Gödde et al. (2020), however, reported that certain Eoarchean rocks from Isua (Greenland) are characterized by Ru isotopic compositions with even greater s-process isotope enrichment than what is documented in the modern BSE. They interpreted this composition as reflecting a mantle source composition that was deficient in late accreted materials and, therefore, representative of the pre-late accretionary mantle. The study concluded that the strongly NC-like, pre-late accretion isotopic composition of the BSE was subsequently modified to that of the modern BSE composition by the late accretion of strongly s-process depleted, most likely CC-type-dominated materials. Given that moderately siderophile Mo in the BSE was not as strongly affected by late accretion as highly siderophile Ru, the Mo and Ru isotopic compositions of the mantle prior to late accretion are expected to provide essentially the same genetic fingerprint. The strongly NC-like Ru isotopic data of the presumed pre-late accretion BSE, therefore, may conflict with the NC-CC mix reflected in the terrestrial Mo isotopic data as reported by Budde et al. (2019).

There are other disagreements in data used to constrain the origin of materials involved in late accretion to Earth. For example, the inferred Ru isotope requirement of a dominant-CC component added by late accretion suggested by Fischer-Gödde et al. (2020) conflicts with the long-lived radiogenic, highly siderophile ¹⁸⁷Re-¹⁸⁷Os isotope system (t_½ = 42 Gyr). The ¹⁸⁷Os/¹⁸⁸Os isotopic composition estimate for the BSE indicates a long-term Re/Os that is similar to NC-type ordinary or enstatite chondrites rather than carbonaceous chondrites (Meisel et al., 2001). Other studies have utilized elemental ratios and mass-dependent isotopic compositions of siderophile elements (e.g., Te, Se) to argue in favor of CC (e.g., Wang and Becker, 2013; Fehr et al., 2018; Varas-Reus et al., 2019) or NC dominance of late accreted materials (e.g., Hellmann et al., 2021).

Given the aforementioned conflicts involved in constraining Earth's late-stage building blocks, this study re-examines the Mo genetic isotope composition of the BSE. Both mass-independent and mass-dependent Mo isotopic data are reported for a range of Archean through to modern terrestrial samples using self-consistent chemical processing techniques and an improved negative thermal ionization mass spectrometry (N-TIMS) method. The new data are combined to generate a revised estimate of the Mo isotopic composition of the BSE. In addition, six iron meteorites are analyzed with these new methods to better constrain the position and slope of the $\mu^{94}\text{Mo vs.}$ $\mu^{95}\text{Mo NC}$ meteorite correlation relative to the BSE, which is necessary to assess the NC vs. CC contributions. Particular attention is given to the main group IAB iron meteorites, which have been used as the anchor for the more s-process-enriched portion of the NC trend that lies closest to prior estimates of the BSE.

2. Samples and Methods

2.1. Samples

To better constrain the mass-independent isotopic composition of Mo

in the BSE, eight Archean, Proterozoic, and Phanerozoic molybdenites, as well as a Phanerozoic whole rock silicate sample, a mid-ocean ridge basalt (MORB), and an estuarine sediment core were analyzed (see S1. Terrestrial sample description and standards). Molybdenite (MoS₂) is an attractive material to interrogate when attempting to constrain the Mo isotopic composition of the BSE. Molybdenum is an essential major element constituent of molybdenite. This makes purification comparatively straightforward by reducing matrix effects that are often present when processing the larger quantities of silicate rocks required for highprecision analysis. Further, molybdenite formation requires the concentration of Mo from a sizeable volume of silicate melt or fluid. Thus, the processes that concentrate Mo in molybdenites may serve to average the mass-independent and mass-dependent Mo isotopic composition of regional samples. Using molybdenites provides a complementary approach to using strictly mantle-derived materials, which may or may not possess genetic anomalies (i.e., Ru isotope compositions from Isua; Fischer-Gödde et al., 2020), include core-derived material (i.e., W isotope compositions in ocean island basalts; e.g., Rizo et al., 2019; Mundl-Petermeier et al., 2020), or be contaminated by Mo during mass production of sample powder (e.g., rock standards; Weis et al., 2006).

The molybdenite samples analyzed here for their mass-independent and mass-dependent isotopic compositions are from the Isua Supracrustal Belt (Greenland, $\sim\!3,810$ Ma), Bushveld Complex (South Africa, $\sim\!2,000$ Ma), Ivigtût (Greenland, 1,248 \pm 25 Ma), Highland Valley (Canada, 209 \pm 2 Ma), Molybdenite Creek (USA, $\sim\!90$ Ma), Komaki (Japan, 64.2 Ma), Mt. Tolman (USA, 61 to 50 Ma), and UR-2 (USA, $\sim\!28.5$ Ma). Also analyzed were Y52 (granodiorite, USA, 91 Ma), a modern Chesapeake Bay sediment core 55(50) (estuarine sediment, USA), and Phoenix MORB (MELPHNX-2-062-003). For more information on these samples, see \$1. Mass-dependent effects are monitored to assess each sample for mass-dependent fractionation effects that can potentially lead to "artificial" (i.e., "spurious") isotopic compositions when combined with instrumental mass fractionation corrections methods (e.g., Budde et al., 2023).

Although there is a large number of Mo isotopic data for meteorites in the literature, the approach used here is to analyze a suite of representative NC meteorites that have been previously shown to have experienced minimal to no exposure to cosmic rays, using self-consistent chemical separation and mass spectrometric procedures. Iron meteorites were chosen to refine the NC μ^{94} Mo vs. μ^{95} Mo trend because they provide the most representative siderophile element composition of their respective parent bodies, given that they are either samples of asteroid cores or large impact-derived melt sheets. They also do not contain acid insoluble phases (e.g., presolar grains), which, if not dissolved, can result in inaccurate bulk compositional analyses (Bermingham et al., 2016). Six iron NC meteorites obtained from the Division of Meteorites, Department of Mineral Sciences, Smithsonian Institution were analyzed: group IAB Campo del Cielo (USNM 5615) and Hope (USNM 3477), group IC Chihuahua City (USNM 853), group IIAB Negrillos (USNM 1222), group IIIAB Costilla Peak (USNM 720), and group IVA Charlotte (USNM 577). The data for these meteorites were teamed with published Mo isotopic data for the NC group IIIE iron meteorite Coopertown (USNM 1003) and ungrouped iron meteorite Lieksa (Geological Survey of Finland), obtained in the same laboratory using self-consistent methodologies.

Internal laboratory Mo solution standards $Alfa\ Aesar^{\text{TM}}\ Specpure^{\text{TM}}$ (i. e., " $Alfa\ Aesar$ "; lot number 32-418803F) and NIST SRM 3134 (lot number 891307) were measured for mass-independent and mass-dependent Mo isotope compositions (S1). Neither standard solution required chemical purification prior to analysis. Mass-independent Mo isotopic data presented here are referenced to the $Alfa\ Aesar$ standard. Repeated measurements of this standard are also used to define the reported long-term precision for the N-TIMS method used. In the absence of an inter-laboratory Mo standard, the mass-independent Mo isotopic composition of NIST SRM 3134 standard was measured to compare the mass spectrometric method to published studies that also report isotopic

data for NIST SRM 3134 (e.g., Budde et al., 2019, 2023; Yobregat et al., 2022). In accordance with published studies, NIST SRM 3134 was used as the reference standard for the Mo mass-dependent isotope measurements. The *Alfa Aesar* Mo standard was measured for mass-dependent Mo isotope compositions to determine the degree of Mo isotope fractionation present in that standard.

2.2. Analytical procedures

At least two issues have hampered the application of the Mo isotopic system to constrain the nature of Earth's late-stage building blocks. First, most previously reported Mo isotopic data for meteoritic and terrestrial samples were obtained by static signal collection mass spectrometric methods (e.g., N-TIMS; Nagai and Yokoyama, 2016, Worsham et al., 2016) and multi-collector inductively coupled plasma mass spectrometry (MC-ICP-MS) (e.g., Budde et al., 2019, 2023). The N-TIMS static methods, however, may be biased by unaccounted-for fractionation effects at the high level of precision required for terrestrial sample analysis. Second, the μ^{94} Mo ν s. μ^{95} Mo correlations for NC and CC materials that have been used to constrain the genetics of Mo in the BSE are defined by linear regressions of data for different materials combined from different studies that used different analytical chemistry procedures and measurement methods. At high precision, such differences in materials and methodologies may lead to inconsistencies in the data, which can translate to variances in the slopes and positions of the NC and CC correlations relative to the BSE estimate. Evidence for this problem may lie in the fact that the relationship between the NC and CC correlations on plots of μ^{94} Mo vs. μ^{95} Mo for cosmochemical materials has oscillated between parallel and non-parallel (Fig. S1), depending on the data used to construct the correlations (i.e., Worsham et al., 2017; Budde et al., 2019; Yokoyama et al., 2019; Spitzer et al., 2020).

Towards these ends, terrestrial and extraterrestrial samples were chemically processed for mass-independent Mo isotopic compositions following the methods of Worsham et al. (2016) and Nagai and Yokoyama (2016), at the Isotope Geochemistry Laboratory, University of Maryland (UMd) (for more details about the analytical methods, see **S2.** Chemical procedures). Using a Thermo Scientific Triton Plus TIMS in negative mode at UMd, the mass-independent Mo isotopic analyses of the samples were performed multiple times for each sample for improved statistics. For this study, a new 3-step multi-dynamic data acquisition method, coupled with rigorous monitoring of fractionation prior to initiating the measurement on the mass spectrometer, was employed to reduce instrumental fractionation effects and improve analytical precision over prior N-TIMS studies that used static collection mode. For more information on the mass spectrometric method and results for standards used in this study, see S3. Mass spectrometry. Long-term precision is reported for the *Alfa Aesar* Mo standard (n = 74) using the multi-dynamic collection routine, with data collected over ~ 2 years (Table 1, Tables S3, and Tables S3, S4). The 2SD variances for the Alfa Aesar standard are $\mu^{92}\text{Mo} \pm 49$, $\mu^{94}\text{Mo} \pm 12$, $\mu^{95}\text{Mo} \pm 8$, $\mu^{97}\text{Mo} \pm 7$, $\mu^{100}\text{Mo} \pm 25$. The 2SE variances for the same standard are $\mu^{92}\text{Mo} \pm 6$, μ^{94} Mo \pm 1, μ^{95} Mo \pm 1, μ^{97} Mo \pm 1, μ^{100} Mo \pm 3. The external precision achieved for the Alfa Aesar Mo standard 94Mo/96Mo (multi-dynamic), ⁹⁵Mo/⁹⁶Mo (multi-dynamic), and ⁹⁷Mo/⁹⁶Mo (multi-dynamic) is improved compared with static N-TIMS studies (e.g., Worsham et al., 2016; Yokoyama et al., 2019) (Fig. 1). The precision for these ratios is similar to the multi-dynamic N-TIMS results for 16 standards measured over 6 months reported by Yobregat et al. (2022), although the present study reports precision for 74 standards that were measured over ~ 2 years. The $^{100}\mathrm{Mo}/^{96}\mathrm{Mo}$ (multi-static) external precision is improved relative to static N-TIMS (Worsham et al., 2016; Yokoyama et al., 2019), but less precise than the multi-dynamic data reported by Yobregat et al. (2022). The external precision achieved for ⁹²Mo/⁹⁶Mo (multi-static) is improved relative to static N-TIMS used by Worsham et al. (2016) and comparable to that reported by Yokoyama et al. (2019). The ⁹²Mo/⁹⁶Mo ratio was not reported by Yobregat et al. (2022).

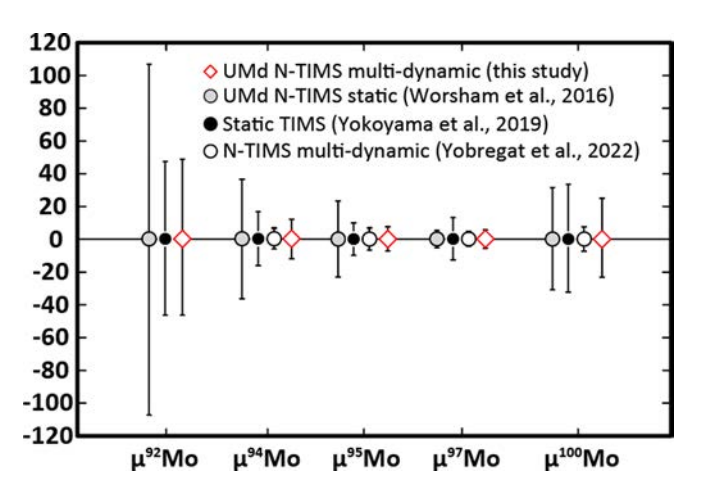


Fig. 1. Comparison of the analytical precision reached in this study compared with Worsham et al. (2016), Yokoyama et al. (2019), and Yobregat et al. (2022). The precision reported by the present study represents repeated multistatic ($\mu^{92}\text{Mo}$ and $\mu^{100}\text{Mo}$) and multi-dynamic ($\mu^{94}\text{Mo}$, $\mu^{95}\text{Mo}$, and $\mu^{97}\text{Mo}$) measurements (n = 74) of the *Alfa Aesar* standard by N-TIMS. The precision Worsham et al. (2016) reported represents repeated static measurements (n = 48) of the *Alfa Aesar* solution standard by N-TIMS. The precision reported by Yobregat et al. (2022) represents repeated multi-dynamic measurements (n = 16) of a purified NIST SRM 3134 standard by N-TIMS. The $^{92}\text{Mo}/^{96}\text{Mo}$ ratio was not reported by Yobregat et al. (2022).

Mass-dependent Mo isotopic compositions were determined for the terrestrial samples and Alfa Aesar Mo standard by the double spike method using a Thermo Scientific Neptune Plus MC-ICP-MS coupled to a Cetac Aridus II desolvating nebulizer at the Department of Earth and Planetary Sciences, Rutgers University. Using solutions of ~ 100 ppb, 100 ratios were collected in static mode, with concurrent monitoring of Zr and Ru. The double spike (97Mo-100Mo) was calibrated against NIST SRM 3134, and the data were reduced using the "double spike toolbox" algorithm of Rudge et al. (2009). Mass-dependent Mo isotopic data are reported as $\delta^{98}\text{Mo}$ and are normalized to NIST SRM 3134. The uncertainty associated with these data represents the 2SE of the 100 ratios collected during an analysis, as each sample was run once. This uncertainty is similar to the 2SD uncertainty associated with three measurements of NIST SRM 3134 (δ^{98} Mo 0 \pm 0.01, n = 3) and Mo metal powder from Johnson Matthey Company (lot D23Y027) (8^{98} Mo -0.20 ± 0.06 , n = 21) that were run during the same analytical campaign, and three rock standards JB-2 (δ^{98} Mo +0.04 \pm 0.07, n = 3), BHVO-2 (δ^{98} Mo -0.17 \pm 0.13, n = 4), and AGV-2 (δ^{98} Mo -0.09 ± 0.05 , n = 4).

3. Results

The mass-independent Mo isotopic composition of the *Alfa Aesar* and NIST SRM 3134 Mo solution standards analyzed here are identical within the reported precision (Table 1). The absence of an offset between the primary *Alfa Aesar* standard and NIST SRM 3134 reported here coincides with what was reported by Budde et al. (2019). The Budde et al. (2019) study, however, did not report lot numbers for their *Alfa Aesar* standard. Although the isotopic composition of *Alfa Aesar*

Table 1Molybdenum isotopic data for standards and terrestrial samples from this study. Isotope ratios are reported as the deviation (in ppm) of the measured ratio relative to the average for repeated analysis of the *Alfa Aesar* Mo solution standard used here. Published data for standards are listed for comparison.

Sample	n	μ ⁹² Μο	±	μ ⁹⁴ Μο	±	μ ⁹⁵ Μο	±	μ ⁹⁷ Μο	±	$\mu^{100} Mo$	±	$\delta^{98} Mo$	±
Standards													
Alfa Aesar (2SD)	74	≡0	49	≡0	12	≡0	8	≡0	7	≡0	25	-0.19	0.03
Alfa Aesar (2SE)	74	≡0	6	≡0	1	≡0	1	≡0	1	≡0	3	-0.19	0.03
NIST SRM 3134 (2SE)	12	0	28	1	9	1	4	0	2	-5	9	$\equiv 0$	0.01
NIST SRM 3134 (95% CI)*	42	-4	5	0	4	1	3	2	2	-1	3		
NIST SRM 3134 (2SD)	16			0	9	0	7	0	4	0	8		
Kanto-Mo (2SD)#	18		39		12		5		9		15		
Δ(Alfa Aesar-3134)		0		-1		-1		0		5		-0.19	
Δ(Alfa Aesar-3134, errors are 2SE) [†]		-1	4	-1	3	0	2	0	2	4	2	-0.58	
Terrestrial samples													
Molybdenites													
Isua (~3,800 Ma) (2SE)	15	-40	24	-22	7	-3	3	12	2	-26	8	+1.37	0.03
Bushveld (~2,000 Ma) (2SE)	12	1	26	-5	8	-4	4	3	2	4	10	+0.04	0.01
Ivigtût (~1,248 Ma) (2SE)	11	15	30	-2	9	-4	3	1	2	12	8	-0.33	0.01
Highland Valley (~209 Ma) (2SE)	8	7	16	6	5	1	2	-5	4	10	3	-1.01	0.02
Molybdenite Creek (~90 Ma) (2SE)	12	-26	25	-15	6	-3	4	5	3	-8	15	+0.15	0.01
Komaki (~64.2 Ma) (2SE)	10	20	33	-1	11	1	4	9	1	2	11	+0.84	0.03
Mt. Tolman (61 to 50 Ma) (2SE)	8	16	19	-5	8	0	4	2	1	12	8	-0.08	0.01
UR-2 (~28.5 Ma) (2SE)	12	-6	29	-7	10	-3	4	4	2	-7	9	+0.11	0.01
Silicate samples													
Y52 (~91 Ma) (2SD)	3	-33	49	-5	12	7	8	6	7	-23	25	+0.01	0.02
Core 55 (present-day) (2SE)	8	-36	20	-7	5	0	2	0	3	-18	9	-0.02	0.05
Phoenix MORB (MELPHNX-2-062-003) (present-day) (2SE)	6	-30	27	-9	5	1	4	6	3	-13	14	+0.53	0.03
BSE composition (2SE)		-12	15	-7	3	-1	3	3	2	-5	9		

For mass-independent Mo isotopic data, sample compositions reflect the average composition of multiple (n) analyses of a single digestion. For individual analyses and associated Alfa Aesar standard composition, see Table S4. The uncertainty associated with sample averages represents the 2SD of the Alfa Aesar standard composition when $n \le 4$ or 2SE of repeated analyses of the samples when $n \ge 5$. n refers to the number of analyses, using a new filament assembly, of purified Mo from a single digestion. The BSE composition was determined by averaging the mean sample compositions of all terrestrial samples (except for molybdenites Isua, Highland Valley, and Komaki) and the error for BSE is the 2SE of the 8 averaged sample compositions. Mass-dependent Mo isotopic data are reported as δ^{98} Mo and are normalized to NIST SRM 3134. All samples were measured once, thus the uncertainty associated with these data represents the 2SE of the ratios collected during an analysis. This uncertainty is similar to the 2SD uncertainty associated with 3 measurements of NIST SRM 3134 run during the same campaign, and three rock standards (JB-2, AVG-2, BHVO-2).

^{*} Data from Budde et al. (2019). 95% CI refers to 95% confidence intervals. Data reported relative to the Alfa Aesar Mo standard used in that study.

Data from Yobregat et al. (2022). Data reported relative to the average for repeated analysis of the "purified once" NIST SRM 3134 standard used in that study.

Data from Yokoyama et al. (2019). Data are from analytical campaign 360R-2, which has the highest precision reported for μ⁹⁵Mo. Data reported relative to the Kanto-Mo standard used in that study.

 $^{^{\}dagger}$ Δ (AA-3134) from Budde et al. (2023).

standards may vary with different lot numbers, the fact that the Alfa Aesar standard is isotopically the same as the NIST SRM 3134 in both the present study and Budde et al. (2019) means that either standard can be used as the point of reference for calculating μ -values. Yobregat et al. (2022) reported data for NIST SRM 3134 but did not measure an Alfa Aesar Mo solution standard. This is not an issue because all samples are referenced to a purified NIST SRM 3134. There are no common standards with Yokoyama et al. (2019).

Most studies reporting the slope and intercept of the NC correlation on plots of μ^{94} Mo ν s. μ^{95} Mo have included the IAB data from Worsham et al. (2017) to anchor the NC regression nearest the origin and, presumably, nearest the BSE composition. Accurate and precise determination of the isotopic composition of IAB main group is, therefore, crucial for defining proportions of NC to CC materials in the BSE. An important aspect of the present study is the re-measurement of two group IAB main group iron meteorites (Campo del Cielo and Hope, chosen because of a lack of Pt or Os isotopic evidence for CRE) using the improved analytical methods presented here, compared to the static N-TIMS study used by Worsham et al. (2017). The Mo isotopic composition of the other iron meteorite pieces analyzed here also did not require CRE correction based on either their Pt isotope compositions measured here (Charlotte, Chihuahua City, Costilla Peak; Table \$5) or reported Os isotopic compositions (Hope, Negrillos, and Campo del Cielo) from those same or closely neighboring pieces (Bermingham et al., 2018; Chiappe, 2023; Chiappe et al., 2023). The Mo isotopic compositions of the iron meteorites reported here are generally similar to published data from other labs for those meteorites (Table 2). For the common samples Campo del Cielo and Hope, a comparison between compositions reported here, Worsham et al. (2017), and Marti et al. (2023), is shown in Table S6. Due to the lower precision reported by Worsham et al. (2017), the new values reported here overlap within uncertainties but are significantly more precise. The composition for Campo del Cielo reported by Marti et al. (2023) overlaps with the composition reported here, except for μ^{92} Mo, which differs by a minimum of 14 ppm.

The uncertainty envelopes (2SE) for nearly all isotopic ratios for the molybdenites and silicate samples overlap within or plot very near the 2SE uncertainty of the long-term precision of the *Alfa Aesar* standard (Fig. 2). Repeated analyses (n = 15) of the Archean Isua (Greenland) molybdenite, however, are characterized by deviations that are well resolved from the standards with average $\mu^{92}\text{Mo}-40\pm24$ (2SE), $\mu^{94}\text{Mo}-22\pm7$, $\mu^{97}\text{Mo}$ 12 \pm 2, $\mu^{100}\text{Mo}-26\pm8$. The $\mu^{95}\text{Mo}$ value of -3 (\pm 3 2SE) of this sample, however, is not resolved from the standard at the 2SE level of precision. Repeated analyses of the following samples are

characterized by small deviations (≥ 1 ppm) in some isotope ratios: Ivigtût $\mu^{100}\text{Mo}$ 12 ± 8 ; Highland Valley $\mu^{97}\text{Mo}$ -5 ± 4 and $\mu^{100}\text{Mo}$ 10 ± 3 ; Molybdenite Creek $\mu^{94}\text{Mo}$ -15 ± 6 and $\mu^{97}\text{Mo}$ 5 ± 3 ; Komaki $\mu^{97}\text{Mo}$ 9 \pm 1; Mt Tolman $\mu^{100}\text{Mo}$ 12 ± 8 ; UR-2 $\mu^{97}\text{Mo}$ 4 \pm 2; Core 55 (50) $\mu^{92}\text{Mo}$ -36 ± 20 , $\mu^{94}\text{Mo}$ -7 ± 5 , $\mu^{100}\text{Mo}$ -18 ± 9 ; and Phoenix MORB $\mu^{94}\text{Mo}$ -9 ± 5 and $\mu^{97}\text{Mo}$ 6 \pm 3.

Although the *Alfa Aesar* Mo solution standard used here has an indistinguishable mass-independent Mo isotopic composition compared to NIST SRM 3134, its mass-dependent Mo isotopic composition ($\delta^{98}\text{Mo}=-0.19\pm0.03$) is slightly fractionated compared to NIST SRM 3134 ($\delta^{98}\text{Mo}\equiv0$) (Table 1). By contrast, the *Alfa Aesar* Mo standard reported by Budde et al. (2023) has a more fractionated mass-dependent Mo isotopic composition ($\delta^{98}\text{Mo}=-0.58$), which that study attributed to kinetic isotope fractionation effects. Most Mo reference standards are purified molybdenite ores or Mo produced as a byproduct of W and Cu production. As the process of ore deposition and purification can generate mass-dependent isotopic shifts, mass-dependent Mo isotopic fractionation coupled with normal mass-independent Mo isotopic compositions can be anticipated.

The mass-dependent Mo isotopic compositions of the terrestrial samples examined here have $\delta^{98}\text{Mo}$ values ranging from -1.01 ± 0.02 (Highland Valley molybdenite) to $+1.37\pm0.03$ (Isua molybdenite). Except for the Komaki molybdenite (+0.84 \pm 0.03), Highland Valley, and Isua molybdenites, all samples cluster within a restricted range with values between -0.5 and +0.5 (Table 1).

4. Discussion

4.1. Molybdenum isotope measurement issues

Most N-TIMS studies have employed static methods to analyze Mo isotopes in terrestrial and extraterrestrial samples (e.g., Nagai and Yokoyama, 2016; Worsham et al., 2016, 2017; Bermingham et al., 2018; Hilton et al., 2019; Yokoyama et al., 2019; Hilton and Walker, 2020; Tornabene et al., 2020, 2023; Chiappe et al., 2023). Although this mass spectrometric method can achieve high precision for Mo isotopic ratios, data reported for repeated analyses of standards and samples can display inter-isotope ratio correlations at the very high levels of precision that are relevant to terrestrial studies. This effect is especially pronounced in plots of μ^{94} Mo vs. μ^{95} Mo. For example, data collected by the repeat analysis of unprocessed Mo solution standards using static N-TIMS display correlated compositions ranging from up to μ^{94} Mo \sim 45 to +45 and μ^{95} Mo \sim 25 to +20 (Fig. 3). Even though the effects in static N-

Table 2Molybdenum isotopic data for iron meteorites. Isotope ratios are reported as the deviation (in ppm) of the measured ratio relative to the average for repeated analysis of the *Alfa Aesar* Mo solution standard used here. Samples did not require CRE correction.

Sample	n	μ ⁹² Μο	±	μ ⁹⁴ Μο	±	μ ⁹⁵ Μο	±	μ ⁹⁷ Μο	±	μ ¹⁰⁰ Μο	±
IC Group											
Chihuahua City	1	94	49	91	12	41	8	26	7	22	25
IAB Group											
Campo del Cielo average	6	-33	25	-2	6	3	1	7	2	-14	11
Hope average	5	15	29	10	4	4	2	5	4	0	20
IIAB Group											
Negrillos	1	159	49	136	12	74	8	43	7	41	25
IIIAB Group											
Costilla Peak	3	141	49	116	12	60	8	32	7	33	25
IIIE Group											
Coopertown ^a	2	106	41	100	14	51	8	21	6	20	22
IVA Group											
Charlotte	5	76	31	75	5	42	4	22	1	17	14
Ungrouped											
Lieksa ^b	3	75	37	79	12	37	8	24	4	5	20

Sample compositions reflect the average composition of multiple (n) analyses of a single digestion. For individual analyses and associated *Alfa Aesar* standard composition, see Table S4. The uncertainty associated with averages represents the 2SD of repeated analyses of the *Alfa Aesar* standard composition when $n \le 4$ or 2SE of repeated analyses of the samples when $n \ge 5$. n refers to the number of analyses, using a new filament assembly, of purified Mo from a single digestion.

^a Data from Chiappe et al. (2023a).

^b Data from Chiappe (2023b).

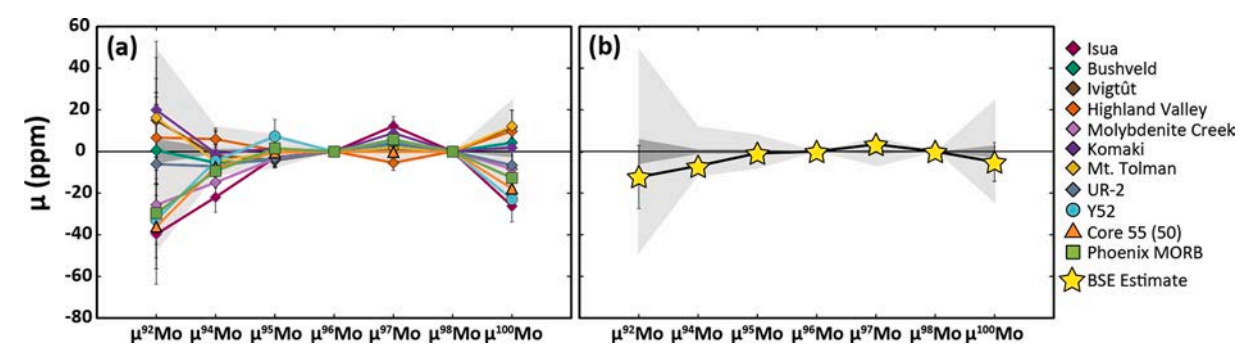


Fig. 2. (a) Plot of averaged μ^i Mo for terrestrial samples listed in Table 1. Sample compositions reflect the average composition of multiple analyses (n) of a single digestion. The uncertainty associated with averages represents the 2SD of the *Alfa Aesar* standard when $n \le 4$ or 2SE of repeated analyses of the samples when $n \ge 5$. The light grey and dark grey fields denote the 2SD and 2SE, respectively, of repeat analyses of the *Alfa Aesar* solution standard (n = 74). (b) The BSE estimate is based on samples (except for Isua, Komaki, and Highland Valley molybdenites) measured in this study. The light grey and dark grey fields denote the 2SD and 2SE, respectively, of repeat analyses of the *Alfa Aesar* solution standard (n = 74).

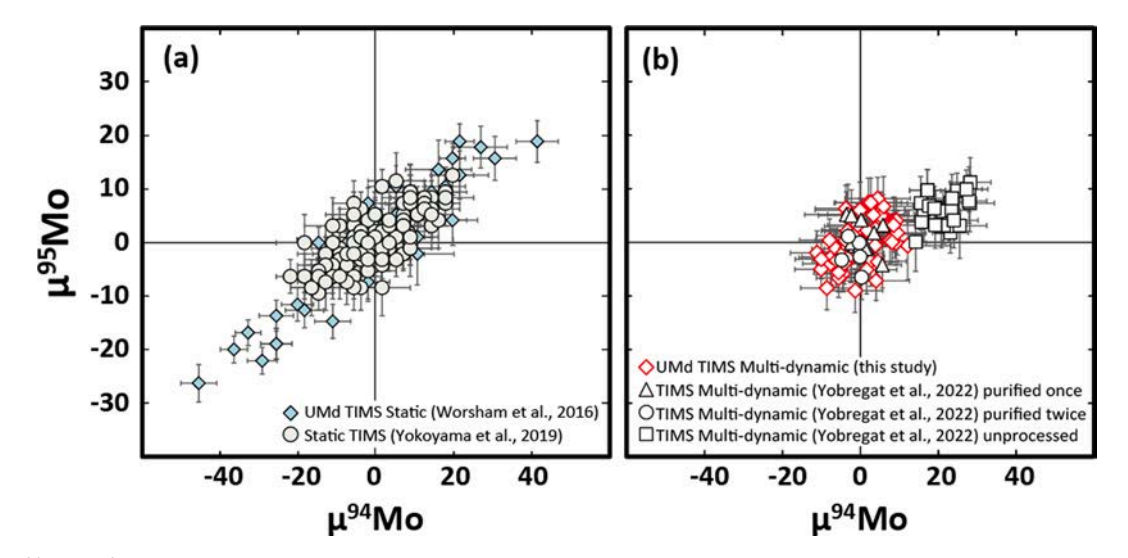


Fig. 3. A plot of μ^{94} Mo vs. μ^{95} Mo for (a) UMd *Alfa Aesar* solution standard using the static N-TIMS method by Worsham et al. (2016) and Yokoyama et al. (2019); and (b) the UMd *Alfa Aesar* solution standard measured using the multi-dynamic N-TIMS methods in the present study and NIST SRM 3134 from Yobregat et al. (2022). The unprocessed NIST SRM 3134 standard data reported by Yobregat et al. (2022) are offset from their "purified once" and "purified twice" NIST SRM 3134 data and the new NIST SRM 3134 data reported here. The offset between the two datasets reported by Yobregat et al. (2022) was concluded by that study to be due to the presence of organic impurities.

TIMS measurements are relatively minor and do not greatly affect sample compositions reported for isotopically anomalous materials (e. g., genetic compositions of meteorites), they become more significant when attempting to determine the composition of the BSE precisely and accurately using the $\mu^{94}\text{Mo}\ vs.\ \mu^{95}\text{Mo}\ plot.$

Commonly in mass spectrometric studies, the isotopic composition of an individual sample is reported as the mean value of multiple analyses. This approach assumes that the averaged ratios accurately reflect the composition of a sample. The presence of inter-isotope ratio correlations in Mo isotope data, however, means that this may not always be a safe assumption. Potentially, these correlations are an important problem given that the genetic characteristics of late-stage accretion to the Earth have previously been determined for Mo through the position of the isotopic composition of the BSE relative to the NC and CC correlation lines on a plot of $\mu^{94} \text{Mo } vs.~\mu^{95} \text{Mo}.$

The data trends observed in Mo isotopic data collected via static N-TIMS methods may be a result of nuclear field shift effects, which is a phenomenon that occurs exclusively during the separation of elements by ion exchange chromatography (Fujii et al., 2006; Budde et al., 2023). The trends could also be an example of "artificial" isotopic compositions that are generated due to the presence of insufficiently corrected chemistry-induced mass-dependent isotope fractionation signatures

(Anbar et al., 2001; Siebert et al., 2001; Budde et al., 2023). The trends observed in static N-TIMS data, however, are unlikely to be predominately caused by these effects because data for unprocessed *Alfa Aesar* (Worsham et al., 2016) and *Kanto-Mo* (Yokoyama et al., 2019) Mo solution standards display the trends (Fig. 3).

Yobregat et al. (2022) reported μ^{94} Mo vs. μ^{95} Mo data for a processed NIST SRM 3134 solution standard that were collected using a multidynamic N-TIMS method, and these data showed a significant reduction in the trend compared to static N-TIMS standard data (e.g., Worsham et al., 2016; Yokoyama et al., 2019) (Fig. 3). This suggests that the primary cause of the trends in static data is, in part, generated by cup biases that are subsequently reduced by using a multi-dynamic method. The residual trends observed in the N-TIMS multi-dynamic data could be caused by measurement uncertainties such as counting statistics and Johnson noise (Andreasen and Sharma, 2009; Dauphas et al., 2014). There may also be minor effects from the insufficient correction of natural fractionation in a standard or sample by the correction schemes employed (i.e., "artificial" isotopic compositions; Budde et al., 2023). Alternatively, the effects may reflect uncorrected isotopic fractionation generated during measurement by the formation of multiple oxide species (Bourdon and Fitoussi, 2020; Yokoyama et al., 2023a).

The present study applied a similar triple peak hop N-TIMS method

to that reported by Yobregat et al. (2022). The main difference between the methods is the cup configuration and the number of measured multidynamic ratios. The present study reports three multi-dynamic ratios (94Mo/96Mo, 95Mo/96Mo, 97Mo/96Mo) compared to the four multidynamic ratios (94Mo/96Mo, 95Mo/96Mo, 97Mo/96Mo, 100Mo/96Mo) reported by Yobregat et al. (2022). The present study also reports multistatic data for 92Mo/96Mo and 100Mo/96Mo. Yobregat et al. (2022) did not report data for 92Mo/96Mo. The configuration reported by Yobregat et al. (2022) also allows for the simultaneous collection of ZrO3, NbO3, and RuO3 species for monitoring interferences on Mo trioxides. The interfering Zr, Nb, and Ru trioxides, however, never reached detectable levels and were, therefore, neglected in that study. These interference species have also not been detected during data collection for the present study; thus, these species were not constantly monitored during the runs.

Here, the magnitude of the μ^{94} Mo vs. μ^{95} Mo correlations in standards and samples is reduced using the multi-dynamic method compared to static N-TIMS data, although trends remain in some of the multi-dynamic data (Fig. 3; Fig. S3 and S4). Future work is needed to further investigate potential causes and corrections that could be employed. Importantly, however, the μ^{97} Mo values for standards and terrestrial samples reported here do not display within measurement or between measurement inter-isotope correlations (Fig. S5). This is likely because this ratio $(^{97}\text{Mo}/^{96}\text{Mo})$ lies between the mass fractionation correction isotopes $(^{98}\text{Mo}/^{96}\text{Mo})$ used in this study, so the correction factor is less than that for ^{95}Mo and, especially, ^{94}Mo . Consistent with this is the observation that $^{97}\text{Mo}/^{96}\text{Mo}$ is the most precisely measured ratio using the multi-dynamic methods presented here and in Yobregat et al. (2022) (Fig. 1).

4.2. Anomalous molybdenum isotopic compositions

The mass-independent Mo isotopic data for the Isua molybdenite are characterized by significant deviations in some isotopic ratios relative to the data for the standards and other samples. The Isua molybdenite sample formed either during the Eoarchean or via subsequent remobilization of Mo from the surrounding Eoarchean rocks. Fischer-Gödde et al. (2020) reported that certain Eoarchean rocks from Isua (West Greenland) are characterized by higher $^{100}\text{Ru}/^{101}\text{Ru}$ and $^{102}\text{Ru}/^{101}\text{Ru}$ ratios than estimates for the Ru isotopic composition of the BSE. That study concluded that the Ru isotopic compositions of these rocks reflect genetic isotope heterogeneity among terrestrial rocks inherited from Earth's building blocks. The cosmochemical relationship between Mo and Ru genetic signatures, coupled with the late-stage accretion histories these elements preserve in the BSE, suggest that corresponding Mo genetic isotopic heterogeneity might also be present in the mantle from which these minerals/rocks were ultimately derived. Consequently, the anomalous Mo isotopic composition of the Isua molybdenite reported here could potentially reflect a genetic isotope heterogeneity among ancient terrestrial rocks, as indicated by Isua Ru isotopic data. The apparent s-process enriched Mo isotopic composition of this molybdenite may correspond to the s-process enriched Ru isotopic signature proposed by Fischer-Gödde et al. (2020).

A mixing computer program ("rsp_mix" notebook) was developed here to assess whether the measured Mo and Ru isotopic compositions of the Isua materials can be reproduced using a mixture of p-process, s-process, and/or r-process compositions, which are the nucleosynthetic stellar sources that contribute material to Mo and Ru (S4. Multicomponent nucleosynthetic isotopic mixing models). This mixing program was verified by reproducing published Mo and Ru isotopic compositions of meteorites. The rsp_mix results confirm that while the Isua Ru isotopic composition can be reproduced by an ~ 30 ppm s-process excess (relative to the s-process contribution that is used to generate the Solar System composition), the Isua Mo isotopic composition reported here cannot be so replicated (Fig. S6). This suggests that the anomalous Mo isotopic composition of the Isua molybdenite

reported here does not reflect a genetic isotope heterogeneity among ancient terrestrial rocks, unlike that reported for the Isua Ru isotopic data.

An alternative explanation for the anomalous isotopic composition of the Isua molybdenite is that a consequence of the insufficient correction of natural fractionation in the sample by the exponential law employed here for the mass spectrometric measurement (i.e., "artificial" isotopic compositions; e.g., Budde et al., 2023). While analytically advantageous for terrestrial studies, molybdenite forms through a variety of processes, including fluid deposition (Bookstrom, 1998). These deposition processes may result in mass-dependent fractionation effects that do not follow the exponential law. Irreversible processes in closed systems, such as Rayleigh distillation, equilibrium fractionation, or a combination, can result in non-linear, mass-dependent isotope fractionation. These types of processes are most likely to occur during fluid deposition, such as the processes that produce molybdenites.

The mechanisms to explain these effects have been previously explored with respect to isotopes of Mo (Budde et al., 2023), Nd (Andreasen and Sharma, 2009), and W (Rizo et al., 2016). To explore this possibility for the Isua molybdenite, calculations that were devised to explore such processes for W isotopes as discussed in Rizo et al. (2016), were adapted for Mo. The independent effects of power, Rayleigh, linear, and equilibrium laws during high-temperature hydrothermal deposition were considered, as they may have led to the formation of the Isua molybdenite. For these calculations, a "true" isotopic composition was established, after which isotopic ratios were modified for various degrees of mass-dependent fractionation that were informed by the measured mass-dependent Mo isotopic composition of the Isua molybdenite, using the correction laws and the isotopes commonly used for normalization. The ratios modified by mass-dependent fractionation were then corrected using the exponential law.

Generally, a good fit to the observed Isua data can be achieved by assuming a depositional fractionation applied to the molybdenite using the Rayleigh fractionation law and an +0.2 %/amu fractionation of ⁹⁸Mo/⁹⁶Mo relative to the *Alfa Aesar* Mo solution standard (Fig. 4). These data also follow the slopes for the non-exponential fractionation reported in Budde et al. (2023), which supports the interpretation that these are indeed "artificial" isotopic compositions. Although the values reported here for most isotopes can be replicated by our models, all models used here fail to reproduce the Isua μ^{97} Mo value of +12 unless the mass-dependent fractionation is substantially increased to ~ 1 %/amu fractionation of 98Mo/96Mo relative to the Alfa Aesar Mo solution standard. This is consistent with the $\delta^{98}\text{Mo}$ +1.37 \pm 0.03 massdependent fractionation measured for this molybdenite (Table 1). This is also consistent with $\delta^{98} Mo_{UMdstd}$ +1.56 \pm 0.03, where $\delta^{98} Mo_{UMdstd}$ here refers to the Isua mass-dependent Mo isotopic composition that is renormalized to the Alfa Aesar standard used to normalize the massindependent Mo isotopic composition. This degree of fractionation, however, would lead to substantially larger negative anomalies in μ^{92} Mo, μ^{94} Mo, μ^{95} Mo, and μ^{100} Mo than what is observed in the Isua molybdenite.

Nevertheless, further evidence of insufficient correction of natural fractionation in a sample by the exponential law may be seen in the $\delta^{98}\text{Mo}$ vs. $\mu^{97}\text{Mo}$ plot of the molybdenites measured here (Fig. 5). This plot is characterized by broadly linear trends with the Isua, Highland Valley, and Komaki samples anchoring the trend. The plots of $\delta^{98}\text{Mo}$ vs. $\mu^{94}\text{Mo}$ and $\mu^{100}\text{Mo}$ display weaker trends, and $\delta^{98}\text{Mo}$ vs. $\mu^{92}\text{Mo}$ and $\mu^{95}\text{Mo}$ plot shows no trend. The remaining samples, however, possess limited mass-dependent fractionation ($\delta^{98}\text{Mo}$ –0.5 to +0.5) and do not display correlations between $\delta^{98}\text{Mo}$ vs. $\mu^{\dot{i}}\text{Mo}$. The fact that the mass-dependent isotopic compositions of Isua, Highland Valley, and Komaki scale with the offset of mass-independent isotopic compositions from the standard suggests that slight yet insufficient correction of natural fractionation in a sample by the exponential law occurred.

Given this and the near-replication of the Mo isotopic composition of the Isua molybdenite, it is concluded that the strong Mo mass-dependent

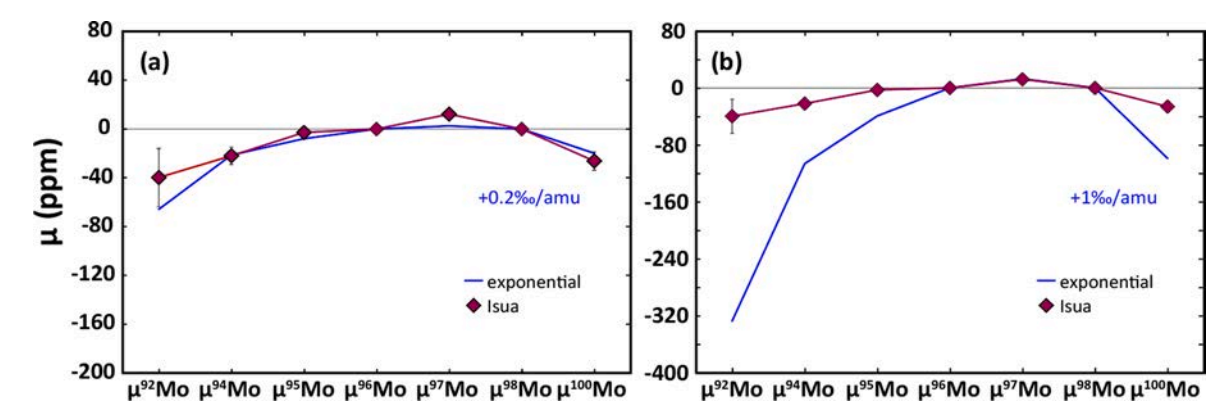


Fig. 4. Models for mass-independent Mo isotopic compositions obtained after correction with exponential law subsequent to natural fractionation of Mo stable isotopes following Rayleigh law mass dependencies (blue line). A generally good fit to the observed Isua data (red symbols) can be achieved by assuming a depositional fractionation applied to the molybdenite using the Rayleigh law and an (a) +0.2 %/amu (respectively) of 98 Mo/ 96 Mo relative to the *Alfa Aesar* Mo solution standard. (b) Depicts the degree of mass-dependent fractionation (+1%/amu) required to reproduce the μ^{97} Mo 12 recorded by the Isua molybdenite.

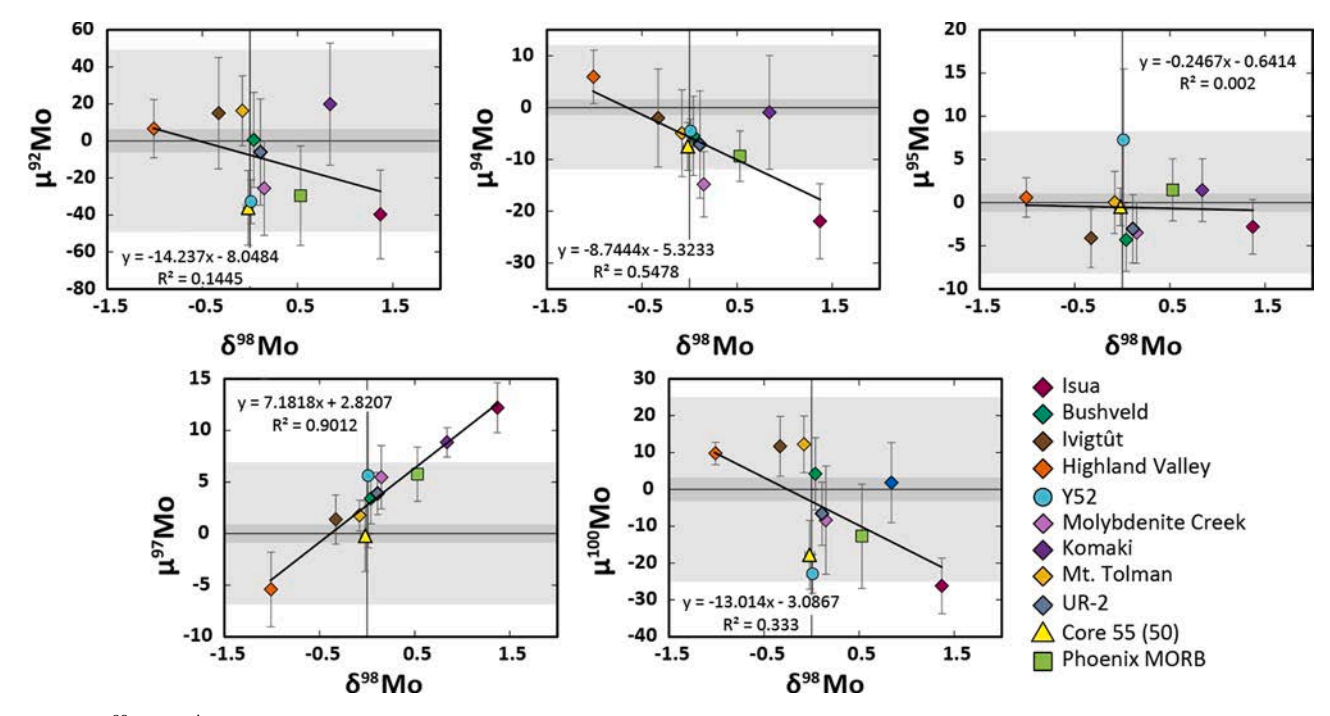


Fig. 5. Plot of δ^{98} Mo vs. μⁱMo for terrestrial samples reported in the present study. The light grey and dark grey fields denote the 2SD and 2SE, respectively, of repeat analyses of the *Alfa Aesar* solution standard. The trends defined by the data (black lines) were calculated using ISOPLOT (Ludwig, 1991).

fractionation recorded by this sample, coupled with insufficient mass fractionation correction, is the most probable cause for the anomalous mass-independent compositions measured. This effect is evident in Highland Valley and Komaki molybdenites; however, it is less pronounced than in Isua. The remaining samples do not show clear evidence of this effect at the resolution of the current study. Why Isua, Highland Valley, and Komaki are unique is unknown; however, it is likely related to fractionation that occurred during fluid deposition.

All samples except for Isua, Highland Valley, and Komaki molybdenites are characterized by a restricted range in mass-dependent isotopic compositions of $\delta^{98}\text{Mo}\sim -0.5$ and +0.5. The values within this range are broadly similar to estimates of the mass-dependent isotopic composition of the BSE (e.g., $\delta^{98}\text{Mo}$ of -0.22 ± 0.06 (2SE) Liang et al., 2017; and -0.21 ± 0.06 (2SE) Greber et al., 2015). The $\delta^{98}\text{Mo}\sim0$ of the molybdenite samples could be a result of multiple different isotopic fractionations. That is, a $\delta^{98}\text{Mo}\sim0$ is not necessarily conclusive evidence of the absence of mass-dependent fractionation. If the near-zero $\delta^{98}\text{Mo}$ composition was a result of multiple different isotopic

fractionations, however, the mass-independent isotopic composition is predicted to be significantly perturbed (Budde et al., 2023). The fact that most of our samples are also characterized by limited variations in all mass-independent Mo isotope ratios indicates that these samples have not undergone multiple mass-fractionation events. The consistency in mass-independent composition for the 8 samples, which display $\delta^{98}\text{Mo}$ between -0.5 and +0.5, indicates that any perturbation in the mass-independent Mo composition caused by uncorrected mass-dependent effects is not significant at the reported level of precision.

4.3. Molybdenum isotopic composition of the BSE

Using molybdenites to estimate the BSE composition provides an important complement to studies using strictly mantle-derived silicate materials. Although some molybdenites display artificial massindependent effects, which may disqualify their application in estimating the BSE composition, most samples do not. Moreover, the use of molybdenites allows circumvention of several issues that arise when

using silicate samples. For example, silicate samples require large sample masses (i.e., several grams) to be processed to isolate sufficient Mo for high-precision analysis. High sample masses can lead to increases in matrix effects in a mass spectrometer, which can be observed as shifts in isotopic composition at high precision. Molybdenites do not suffer from these issues because they are highly concentrated in Mo, thus little material is required for digestion. Also, several of the rock standards commonly used for interlaboratory comparisons have been contaminated by Mo during preparation (e.g., BCR-2 and BHVO-2; Weis et al. 2006) as a result of the use of metal grinding devices with comparatively high Mo concentrations. Such contamination may disqualify these materials from being used to estimate the BSE composition. Moreover, mantle-derived materials may possess genetic anomalies (i.e., Ru isotope compositions in Eoarchean rocks from Greenland; Fischer-Gödde et al., 2020), or include core-derived material representing an earlier phase of Earth's accretion (i.e., as may be evidenced by ¹⁸²W isotope compositions in ocean island basalts; e.g., Rizo et al., 2019; Mundl-Petermeier et al., 2020). Although molybdenites and silicate samples can both display limitations in their application to estimating the BSE, using these materials in concert is likely the most robust approach to estimating the BSE composition at this time.

Collectively, our new results indicate little variation in massindependent Mo isotopic compositions among all samples examined by this study, except for the Isua, Highland Valley, and Komaki molybdenites. Given the diverse geological natures of the samples examined, together with the consistency of the isotopic compositions obtained for the multiple samples, we conclude that the averaged ratios of the 8 samples least affected by mass-dependent effects are likely to be representative of the BSE. Based on these samples (Bushveld, Ivigtût, Molybdenite Creek, Mt. Tolman, UR-2, Y-52, Core 55, Phoenix MORB), the resulting average μ -values and 2SE uncertainties for the BSE are $\mu^{92} Mo~-12~\pm~15,~\mu^{94} Mo~-7~\pm~3,~\mu^{95} Mo~-1~\pm~3,~\mu^{97} Mo~3~\pm~2,$ and μ^{100} Mo -5 ± 9 (Table 1 and Fig. 2). Except for minimum 4 ppm deviation in μ^{94} Mo, these values with uncertainties are unresolved from the 2SE uncertainties for the Alfa Aesar and NIST SRM 3134 standard ratios. If Highland Valley and Komaki molybdenites are included in the BSE estimate, minimal shifts occur with the resulting the average μ -values and 2SE uncertainties becoming $\mu^{92}\text{Mo} -7 \pm 14$, $\mu^{94}\text{Mo} -5 \pm 3$, $\mu^{95}\text{Mo}$ $0\pm2,\,\mu^{97}Mo~3\pm3,$ and $\mu^{100}Mo~-5\pm8.$

In comparison to our new BSE estimate (without Isua, Highland Valley, and Komaki), Budde et al. (2019) estimated the BSE as μ^{92} Mo 8 \pm 13, μ^{94} Mo 4 \pm 6, μ^{95} Mo 10 \pm 4, μ^{97} Mo 6 \pm 2, and μ^{100} Mo -7 \pm 4 (2SE uncertainties). The only resolved discrepancies between the values obtained for the different samples by the two studies are for μ^{94} Mo (which differ by a minimum of 2 ppm) and μ^{95} Mo (which differ by a minimum of 4 ppm). Values for μ^{92} Mo, μ^{97} Mo, and μ^{100} Mo overlap within uncertainties. The presence of minor uncorrected mass fractionation effects in one or both datasets is a likely reason for a different BSE μ^{94} Mo νs . μ^{95} Mo isotopic estimate of the present study compared to Budde et al. (2019, 2023), but it could also reflect some differences in the geological materials examined. It is noted that the rsp_mix modeling program developed here cannot reproduce the $\mu^{94}Mo$ and $\mu^{95}Mo$ BSE compositions reported by Budde et al. (2019), which suggests that this composition is not a result of a combination of known p-, s-, r-process Mo compositions (Fig. S6). In the future, a considerably greater number of samples with diverse origins should be analyzed to further refine the BSE estimate. These studies should combine mass-independent and massdependent compositional analyses to monitor for "artificial" isotopic compositions induced when strongly mass-fractionated compositions are combined with instrumental mass-fractionation correction methods.

4.4. μ^{94} Mo vs. μ^{95} Mo NC-CC correlations

Mass-independent Mo isotope variations in meteorites have been widely used to examine genetic contributions to various planetary materials (Dauphas et al., 2002a, 2004; Burkhardt et al., 2011; Budde et al.,

2016; Worsham et al., 2017; Poole et al., 2017; Bermingham et al., 2018; Yokoyama et al., 2019; Brennecka et al., 2020; Marti et al., 2023). Some $\delta^{98}\text{Mo}$ compositions of iron meteorites have been reported by Burkhardt et al. (2014), and they show little variation ranging from $\delta^{98}\text{Mo}-0.20\pm0.07$ to $+0.22\pm0.03$. As these compositions are within $\delta^{98}\text{Mo}\pm0.5$, it is likely that the mass-independent Mo isotopic variations among iron meteorite data are not significantly affected by uncorrected mass-dependent fractionation effects outside the levels of precision reached in this study. Thus, they are not considered further here.

The plot of μ^{94} Mo vs. μ^{95} Mo has been especially useful for determining NC or CC genetics for iron meteorites and pallasites (Worsham et al., 2017; Kruijer et al., 2017, 2022; Spitzer et al., 2021). Although nearly all meteorites examined to date plot along either NC or CC correlations, the ungrouped iron meteorite Nedagolla was found to have an isotopic composition that falls between the two correlation lines (Spitzer et al., 2021). Its position between the two lines was interpreted to indicate a mixed genetic heritage, and the lever rule, coupled with the assumption that the NC and CC trends are parallel, was applied to constrain the proportion of NC vs. CC material. The approach has also been taken to determine the mixed NC-CC genetics of late-stage accretion to Mars (Burkhardt et al., 2021).

Utilization of the μ^{94} Mo vs. μ^{95} Mo plot to define the proportion of NC vs. CC material added to the BSE during late-stage accretion requires precise constraints on the BSE estimate, but also the positions and slopes of NC, and possibly CC, correlations. To date, most published NC and CC slopes have been determined by linear regression of data for iron, stonyiron, and stony meteorites, and in some cases, meteorite components and primitive meteorite leachates (e.g., Budde et al., 2019, 2023). Most of the variations in isotopic compositions on the μ^{94} Mo vs. μ^{95} Mo plot align with predictions of variability in s-process componentry (Dauphas et al., 2002a, 2004; Burkhardt et al., 2011; Budde et al., 2016; Worsham et al., 2017; Poole et al., 2017).

Most data compilations combine data collected using different techniques, many of which have been collected by static N-TIMS and MC-ICP-MS methods (e.g., Budde et al., 2016, 2019; Worsham et al., 2017; Poole et al., 2017; Spitzer et al., 2020). The compilations often use silicate samples and stony-irons, even though these samples do not provide as robust an average of the siderophile genetic composition of a parent body as iron meteorites. Many samples used in compilations have also been carefully evaluated and corrected for CRE effects.

To revisit the NC trend, the new data generated for six iron meteorites were regressed using ISOPLOT (Ludwig, 1991) (Fig. 6). The regression yields a slope for $\mu^{94} Mo~\nu s.~\mu^{95} Mo~of~0.517 \pm 0.042$ and a yintercept (for μ^{94} Mo = 0) of 1 \pm 2. The slope and intercept coincide with the values of 0.488 \pm 0.085 and -6 \pm 6 reported by Yokoyama et al. (2019) for a suite of NC meteorites that included new data and data compiled from the literature for ordinary, enstatite, and rumuruti chondrites, acapulcoites, lodranites, winonaite, and CRE-corrected irons. By contrast, Budde et al. (2019) reported a steeper slope of 0.596 ± 0.008 and an intercept of -9 ± 2 . The regression of Budde et al. (2019) included new and compiled data for NC iron meteorites, ordinary, enstatite, and rumuruti chondrites, a variety of NC achondrites, as well as data for a series of leachates from an L3.2 chondrite and an H3.3 chondrite. Because of the large ranges in isotopic compositions, the leachate data were particularly important for establishing the slope and achieving the high precision reported by that study for the regression of the NC data.

The main cause for the difference in slopes determined for the present study and that of Budde et al. (2019) is the inclusion of leachates in the regression reported by that study. If leachates are excluded from the Budde et al. (2019) regression dataset, the NC slope becomes shallower (0.528 \pm 0.050), which is the same within error as the NC slope reported here, with an intercept of -6 ± 4 . Using a similar dataset to Budde et al. (2019) but excluding leachate data, Spitzer et al. (2020) reported a slope of 0.528 \pm 0.045 (which is the same within error as the NC slope reported here) and an intercept of -6 ± 4 . Further, if the data for IAB-MG

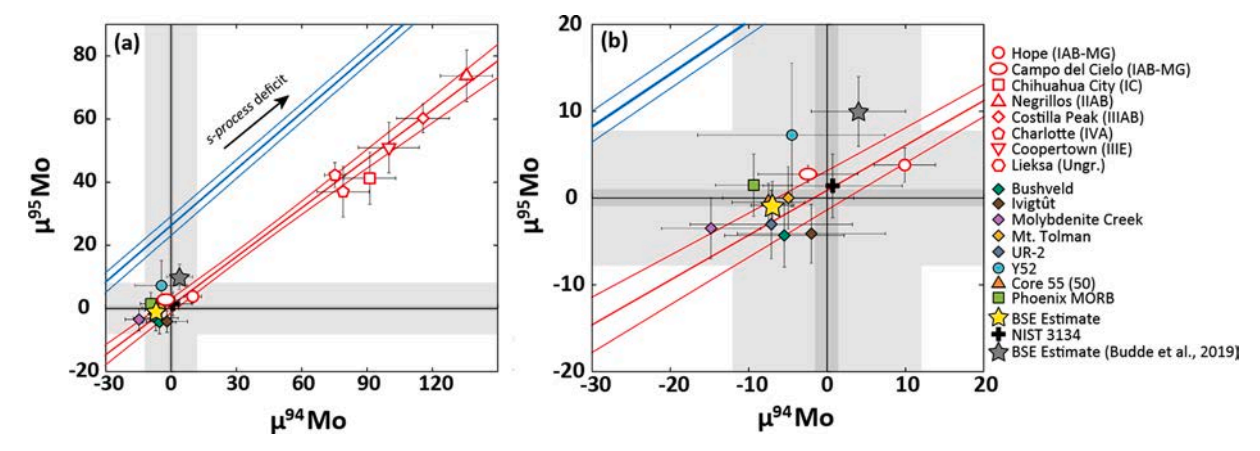


Fig. 6. (a) A plot of μ^{94} Mo vs. μ^{95} Mo for iron meteorite and terrestrial data determined using multi-dynamic N-TIMS in the present study (Table 1). (b) is an enlarged scale version of (a). The NC linear regression and error envelopes are calculated from the NC meteorite groups listed in Table 1 using ISOPLOT. The CC linear regression was taken from Budde et al. (2019). The BSE estimate from Budde et al. (2019) is shown for comparison. The light grey and dark grey fields represent the 2SD and 2SE values, respectively, for the Alfa Aesar solution standard analyses.

irons, taken from Worsham et al. (2017) in the data compilation used by Spitzer et al. (2020), are replaced with the improved average for that group from the present study, the slope, and intercept for the NC line change to 0.476 ± 0.030 and -1 ± 2 , respectively, which are identical to the slope and intercept obtained for the present study.

Although the inclusion of leachate data to construct NC and CC correlations leads to greater precision of the correlations, there are potential issues associated with this approach (for further discussion, see S5. Construction of NC and CC μ^{94} Mo vs. μ^{95} Mo correlations and estimating late-stage accretion componentry). Given the extreme isotopic compositions of some leachates (>100 ppm deviation from normal), these materials have a disproportional influence on the slopes of NC and CC correlations. Their inclusion has been justified by the fact that leachates are considered to sample presolar components that collectively define bulk sample genetic anomalies (Dauphas et al., 2004). It is unknown, however, if the isotopic composition of a leachate represents a single type of presolar component or a mixture of multiple components. Moreover, the elemental concentration in a presolar component is not well constrained via leaching because it is unknown if the element concentration of the leachate represents a single type of presolar component. How influential a leachate's presumed presolar componentry is with respect to defining the genetic composition of a bulk sample, and the parent body, is similarly not well constrained. Thus, using leachates to construct the NC and CC correlations may result in slopes that are not representative of the true variations between NC parent bodies.

To circumvent these issues when revisiting the NC correlation, this study uses isotopic data collected only from iron meteorites, using the self-consistent analytical methods presented here. For a siderophile element like Mo, iron meteorites likely provide the best average composition of the iron-loving elements in a parent body, given they are either samples of asteroid cores or large impact-derived melt sheets. This avoids issues such as the selective mobilization of presolar phases via aqueous or thermal alteration, which have been explanations for unusual nucleosynthetic isotope compositions measured for Os and Mo isotopes in ureilites and stony carbonaceous chondrites (Yokoyama et al., 2011, 2023; Goderis et al., 2015; Nakanishi et al., 2023). The error envelope of the NC μ^{94} Mo vs. μ^{95} Mo slope obtained here coincides with slopes defined by presolar mainstream SiC grains (~93 % of total SiC grains; Amari, 2014) isolated from the Murchison (CM2) meteorite reported by Nicolussi et al. (1998) and Stephan et al. (2019) (Fig. S7). The error envelope of the NC slope obtained here, however, does not coincide with that of mainstream SiC grains reported by Barzyk et al. (2007) and Liu et al. (2017).

The variation in $\mu^{94}\text{Mo}$ vs. $\mu^{95}\text{Mo}$ slopes between the SiC grain

studies may reflect different populations of grains present in the different grain fractions examined by each study (grain fraction KJH by Nicolussi et al., 1998; Barzyk et al., 2007; grain fraction KJG of KJ separate by Stephan et al., 2019; and a unique grain fraction by Liu et al., 2017). Alternatively, it could reflect the analytical developments in the measurement of individual presolar grains. The most recent of these studies (Stephan et al., 2019) used the Chicago Instrument for Laser Ionization (CHILI) and reported that the broader distribution and differences in y-intercepts between their measurements and those of Nicolussi et al. (1998) and Barzyk et al. (2007) could be explained by lesscontrolled measurement conditions during resonance ionization that were used in prior work. Stephan et al. (2019) also noted that the analyses reported by Liu et al. (2017) had larger statistical uncertainties due to low count rates. Moreover, the SiC grains analyzed for Mo isotopes were extracted from carbonaceous chondrites. The difference in slope between the NC line and slopes defined by presolar mainstream SiC grains could be because the SiC grains extracted from CC meteorites have a slightly different s-process composition compared to NC meteorites.

No CC materials were analyzed for this study. Yokoyama et al. (2019) reported a slope and intercept for CC meteorites of 0.600 \pm 0.030 and 26 \pm 6, respectively, based on data for bulk carbonaceous chondrites and CRE-corrected data for CC iron meteorites (Fig. S7). Budde et al. (2019) reported an essentially identical slope 0.596 \pm 0.006 and intercept of 26 \pm 2, using CRE-corrected data for CC iron meteorites, stony-irons and bulk carbonaceous chondrites. These CC slopes coincide with those determined from Mo isotope measurements of presolar mainstream SiC grains, except that reported by Liu et al. (2017) (Fig. S7).

If the slopes of the NC trend without leachates in the present study and the CC trend of Yokoyama et al. (2019) are correct, then the NC and CC correlations are not parallel. Moreover, both the bulk meteorite NC and CC slopes are shallower than the slopes determined using main-stream SiC grains. The differences in $\mu^{94}\text{Mo}$ vs. $\mu^{95}\text{Mo}$ slopes between the bulk meteorite samples and slopes generated from SiC data may reflect different populations of presolar grains in the reservoirs sampled by NC and CC meteorites.

4.5. Assessment of the relative proportion of NC and CC preserved in the

Utilizing the relationship between μ^{94} Mo ν s. μ^{95} Mo in meteorites and the BSE has provided an elegant way to assess the proportions of NC and CC materials in the BSE independent of the absolute isotopic compositions of Earth's building blocks. The new Mo isotope results for the BSE

estimate, combined with the revision to the slope of the NC meteorite correlation, however, leads to a different conclusion regarding the genetic contributions to Mo during late-stage accretion to Earth. The new results, if accurate, reveal $\mu^{94}\text{Mo}$ vs. $\mu^{95}\text{Mo}$ values for BSE that overlap with the error envelop of the NC correlation reported herein (Fig. 6). Consequently, there is no requirement for a significant CC contribution to Mo in the BSE, although the results are permissive of a minor proportion (<10 %) of CC contribution which would be sufficient to move the BSE composition slightly off the NC line but remain within the error envelope of the slope. The apparent lack of parallel correlations between NC and CC trends means that even if the $\mu^{94}\text{Mo}$ vs. $\mu^{95}\text{Mo}$ BSE value is accurately and precisely constrained, the proportions of NC relative to CC cannot be geometrically ascertained from these data, given uncertainties in the compositions of the endmember mixing components.

Given the analytical issues surrounding 94Mo/96Mo and 95Mo/96Mo data, an alternative means for investigating the genetic Mo contributors to the BSE is to consider its μ^{97} Mo value. This ratio is analytically advantageous for examining genetic mixing. Unlike 94Mo/96Mo and ⁹⁵Mo/⁹⁶Mo ratios, ⁹⁷Mo/⁹⁶Mo ratios do not exhibit fractionation trends during standard or sample analysis by N-TIMS, nor do the final ratios show variable fractionation trends among repeated standard and sample analysis. The ⁹⁷Mo/⁹⁶Mo ratio is also the most precisely determined of the Mo isotopic ratios when measured by N-TIMS. Furthermore, μ^{97} Mo is a sensitive tracer of nucleosynthetic isotope anomalies, and the NC or CC classification of meteoritic material is clearly distinguished using μ⁹⁷Mo compositions (Fig. 7). Isotopes ⁹⁶Mo, ⁹⁷Mo, and ⁹⁸Mo are synthesized by the s-process and r-process, while 92 Mo and 94 Mo are dominantly synthesized by the p-process. Thus, unlike μ^{92} Mo and μ^{94} Mo, μ^{97} Mo is less sensitive to the varying contribution of *p*-nuclides (92Mo and 94Mo). This is advantageous if the NC-CC dichotomy of Mo isotopes is dominantly controlled by the varying contribution of s- and possibly r-nuclides (e.g., Budde et al., 2016; Worsham et al., 2017; Kruijer et al., 2017; Poole et al., 2017; Stephan and Davis, 2021).

The proportions of NC and CC materials in the BSE cannot be used to independently assess the absolute isotopic compositions of Earth's building blocks by solely using the $\mu^{97}\text{Mo}$ composition. Nevertheless, an NC-dominated BSE composition is indicated by all Mo isotope ratios reported here ($\mu^{92}\text{Mo},~\mu^{94}\text{Mo},~\mu^{95}\text{Mo},~\mu^{97}\text{Mo},~\mu^{100}\text{Mo})$ as the BSE composition falls within the NC field for each isotope ratio (Fig. 7). The Mo isotopic composition of the BSE is the furthermost removed from any known CC iron meteorites, such that there is no overlap with CC materials. For there to then be a nearly 50:50 mix of NC and CC in the BSE,

as concluded by Budde et al. (2019), there would have to be a major inner Solar System component with strongly negative $\mu^{92} \text{Mo}, \ \mu^{94} \text{Mo}, \ \mu^{95} \text{Mo}, \ \mu^{97} \text{Mo}, \ \text{and} \ \mu^{100} \text{Mo}$ isotopic compositions (i.e., s-process enriched) to balance out the large CC contribution. Such a composition is yet to be reported for any bulk material.

The inference that NC components dominated late-stage accretion is in good agreement with the inferred Ru isotopic composition for the prelate accretion and the BSE (Bermingham and Walker, 2017; Fischer-Gödde et al., 2020; Worsham and Kleine, 2021). It is also consistent with the NC-like $\mu^{183}W$ isotopic composition of the BSE, given that all CC meteorites are characterized by enrichments in ^{183}W compared with terrestrial. Tungsten, like Mo, is a moderately siderophile element whose isotopic composition is also likely dominated by materials accreted to Earth during its final 10 to 20 wt% of growth. The conclusion of dominantly NC accretion during the late stages of Earth's accretion implies that the putative Moon-forming giant impactor, termed Theia, was likely NC in nature and presumptively originated from materials formed in the inner Solar System.

If the common assumption that CC materials originated in the wetter outer portion of the protoplanetary disk is correct, the observations reported here suggest that the Moon-forming event, which likely coincided with final core formation, was not a major supplier of water to the planet. Nevertheless, the conclusion of a dominant NC component during the final 10 to 20 wt% of Earth accretion does not preclude an interpretation of minor CC additions during this period, such as has been suggested by the isotopic compositions of other elements for the final 0.5 to 1 wt% addition to Earth's mass by late accretion (Fischer-Gödde et al., 2020; Wang and Becker, 2013; Varas-Reus et al., 2019).

5. Conclusions

The new Mo isotopic BSE estimate reported here indicates a dominant NC character of Earth's building blocks that accreted during final core formation, although it is permissive of a small (<10 %) CC component. The relative position of BSE to NC-CC lines on a μ^{94} Mo vs. μ^{95} Mo plot, however, depends on multiple analytical factors, which make it challenging to infer the percentages of NC vs. CC accreted to Earth using this approach. The discrepancies between this BSE composition and prior estimates may reflect differences in the analytical methods employed or the materials studied. The μ^{97} Mo isotopic composition of the BSE may be a more reliable ratio to assess NC vs. CC compositions because it is not adversely affected by analytical

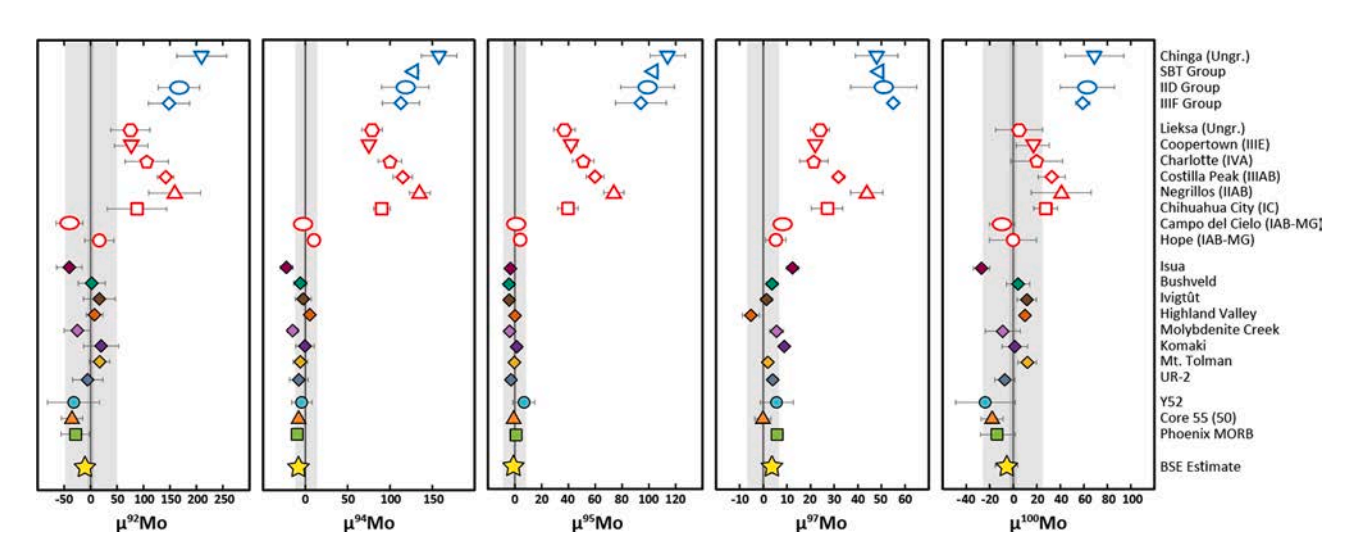


Fig. 7. Multi-dynamic Mo isotopic data for terrestrial samples and NC iron meteorites reported in the present study. Uncertainties for individual analyses represent the 2SD of repeated analyses of the *Alfa Aesar* laboratory standard. The uncertainty associated with averages represents the 2SD of the *Alfa Aesar* standard when $n \le 4$, or 2SE of repeated analyses of the samples when $n \ge 5$. The CC iron meteorite data are from Worsham et al. (2019); Hilton et al. (2019); Yokoyama et al. (2019); Chiappe et al. (2023), all collected via N-TIMS.

challenges. As with μ^{94} Mo vs. μ^{95} Mo, the μ^{97} Mo estimate for BSE provides no evidence for a significant CC component during late-stage accretion. The finding of an NC-dominated accretion during the late-stage of Earth's accretion implies that the putative Moon-forming giant impactor was NC in nature and presumptively originated from materials formed in the inner Solar System. If the interpretation that CC materials originated in the wetter outer portion of the Solar nebula is correct, then these results suggest that late-stage accretion may not have provided the bulk of Earth's water.

CRediT authorship contribution statement

K.R. Bermingham: Writing – review & editing, Writing – original draft, Validation, Software, Methodology, Investigation, Funding acquisition, Conceptualization. H.A. Tornabene: Writing – review & editing, Writing – original draft, Validation, Methodology, Investigation. R.J. Walker: Writing – review & editing, Writing – original draft, Validation, Methodology, Investigation, Funding acquisition, Conceptualization. L.V. Godfrey: Writing – review & editing, Investigation. B. S. Meyer: Writing – review & editing, Software, Methodology, Investigation. P. Piccoli: Writing – review & editing, Resources. S.J. Mojzsis: Writing – review & editing, Resources.

Declaration of competing interest

The authors declare that they have no known competing financial interests or personal relationships that could have appeared to influence the work reported in this paper.

Acknowledgments

We thank Associate Editor Z. Wang for his guidance during review. We further thank G. Budde, M. Fischer-Gödde, and an anonymous reviewer for their helpful and thorough reviews. K.R.B. acknowledges support from NSF grants EAR 2220922 and 2051577, and NASA Emerging Worlds grant 80NSSC20K0997. R.J.W acknowledges support from NSF grant EAR 2020029 and NASA Emerging Worlds grant 80NSSC20K0335. S.J.M. was supported by the HUN-REN Research Centre for Astronomy and Earth Sciences and the PHAB Centre at the University of Oslo (Norway). S.J.M. acknowledges support from the Alexander von Humboldt Stiftung for a Visiting Research Professorship at the University of Jena (Germany) during the preparation of this manuscript. We thank T. McCoy and C. Corrigan (Smithsonian Institution National Museum of Natural History, US) for providing us with the meteorite samples. We thank L. Hale (Smithsonian Institution National Museum of Natural History, US) for providing Bushveld and Ivigtût molybdenites samples, P. Candela (University of Maryland) for providing the molybdite sample Komaki, V. Finlayson (University of Maryland) for providing the Phoenix MORB, and G. Helz for providing the sediment core. We are grateful to A. Patel (Rutgers University) for early contributions towards deriving the multicomponent nucleosynthetic isotopic mixing calculations.

Appendix A. Supplementary material

Supplementary material to this article can be found online at htt ps://doi.org/10.1016/j.gca.2024.11.005.

References

- Amari, S., 2014. Recent progress in presolar grain studies. Mass Spectrom (Tokyo) 3, S0042–S.
- Anbar, A.D., Knab, K.A., Barling, J., 2001. Precise Determination of Mass-Dependent Variations in the Isotopic Composition of Molybdenum Using MC-ICP-MS. Anal. Chem. 73, 1425–1431.

- Andreasen, R., Sharma, M., 2009. Fractionation and mixing in a thermal ionization mass spectrometer source: Implications and limitations for high-precision Nd isotope analyses. Int. J. Mass Spectrom. 285, 49–57.
- Archer, G.J., Budde, G., Worsham, E.A., Stracke, A., Jackson, M.G., Kleine, T., 2023.
 Origin of ¹⁸²W anomalies in ocean island basalts. Geochem. Geophys. Geosyst. 24.
- Barzyk, J.G., Savina, M.R., Davis, A.M., Gallino, R., Gyngard, F., Amari, S., Zinner, E., Pellin, M.J., Lewis, R.S., Clayton, R.N., 2007. Constraining the ¹³C neutron source in AGB stars through isotopic analysis of trace elements in presolar SiC. Meteorit. Planet. Sci. 42, 1103–1119.
- Bermingham, K.R., Mezger, K., Scherer, E.E., Horan, M.F., Carlson, R.W., Upadhyay, D., Magna, T., Pack, A., 2016. Barium isotope abundances in meteorites and their implications for early Solar System evolution. Geochim. Cosmochim. Acta 175, 282–298
- Bermingham, K.R., Walker, R.J., 2017. The ruthenium isotopic composition of the oceanic mantle. Earth Planet. Sci. Lett. 474, 466–473.
- Bermingham, K.R., Worsham, E.A., Walker, R.J., 2018. New insights into Mo and Ru isotope variation in the nebula and terrestrial planet accretionary genetics. Earth Planet. Sci. Lett. 487, 221–229.
- Bookstrom A. A. (1998) Molybdenum. In Geochemistry Springer Netherlands, Dordrecht. pp. 411–413.
- Bourdon, B., Fitoussi, C., 2020. Isotope fractionation during condensation and evaporation during planet formation processes. ACS Earth Space Chem. 4, 1408, 1423
- Brasser, R., Mojzsis, S.J., 2020. The partitioning of the inner and outer Solar System by a structured protoplanetary disk. Nat. Astron 4, 492–499.
- Brasser, R., Dauphas, N., Mojzsis, S.J., 2018. Jupiter's influence on the building blocks of mars and earth. Geophys. Res. Lett. 45, 5908–5917.
- Brennecka, G.A., Burkhardt, C., Budde, G., Kruijer, T.S., Nimmo, F., Kleine, T., 2020. Astronomical context of Solar System formation from molybdenum isotopes in meteorite inclusions. Science 370, 837–840.
- Budde, G., Burkhardt, C., Brennecka, G.A., Fischer-Gödde, M., Kruijer, T.S., Kleine, T., 2016. Molybdenum isotopic evidence for the origin of chondrules and a distinct genetic heritage of carbonaceous and non-carbonaceous meteorites. Earth Planet. Sci. Lett. 454, 293–303.
- Budde, G., Burkhardt, C., Kleine, T., 2019. Molybdenum isotopic evidence for the late accretion of outer Solar System material to Earth. Nat. Astron 3, 736–741.
- Budde, G., Tissot, F.L.H., Kleine, T., Marquez, R.T., 2023. Spurious molybdenum isotope anomalies resulting from non-exponential mass fractionation. Geochemistry 126007.
- Burkhardt, C., Kleine, T., Oberli, F., Pack, A., Bourdon, B., Wieler, R., 2011. Molybdenum isotope anomalies in meteorites: Constraints on solar nebula evolution and origin of the Earth. Earth Planet. Sci. Lett. 312, 390–400.
- Burkhardt, C., Hin, R.C., Kleine, T., Bourdon, B., 2014. Evidence for Mo isotope fractionation in the solar nebula and during planetary differentiation. Earth Planet. Sci. Lett. 391, 201–211.
- Burkhardt, C., Spitzer, F., Morbidelli, A., Budde, G., Render, J.H., Kruijer, T.S., Kleine, T., 2021. Terrestrial planet formation from lost inner solar system material. Sci. Adv. 7, eabj7601.
- Chiappe, E., 2023. Genetics, ages, and chemical compositions of the group IIIE iron meteorites and the iron meteorite lieksa. University of Maryland. Masters thesis.
- Chiappe, E.M., Ash, R.D., Walker, R.J., 2023. Age, genetics, and crystallization sequence of the group IIIE iron meteorites. Geochim. Cosmochim. Acta 354, 51–61.
- Chou, C.-L., 1978. Fractionation of siderophile elements in the Earth's upper mantle. Proc. Lunar Planet. Sci. Conf. 9th, 219–230.
- Dauphas, N., 2017. The isotopic nature of the Earth's accreting material through time. Nature 541, 521–524.
- Dauphas, N., Marty, B., Reisberg, L., 2002a. Molybdenum evidence for inherited planetary scale isotope heterogeneity of the protosolar nebula. Astrophys J 565, 640–644.
- Dauphas, N., Marty, B., Reisberg, L., 2002b. Molybdenum nucleosynthetic dichotomy revealed in primitive meteorites. Astrophys J 569, L139–L142.
- Dauphas, N., Davis, A.M., Marty, B., Reisberg, L., 2004. The cosmic molybdenum-ruthenium isotope correlation. Earth Planet. Sci. Lett. 226, 465–475.
- Dauphas, N., Chen, J.H., Zhang, J., Papanastassiou, D.A., Davis, A.M., Travaglio, C., 2014. Calcium-48 isotopic anomalies in bulk chondrites and achondrites: Evidence for a uniform isotopic reservoir in the inner protoplanetary disk. Earth Planet. Sci. Lett. 407, 96–108.
- Fehr, M.A., Hammond, S.J., Parkinson, I.J., 2018. Tellurium stable isotope fractionation in chondritic meteorites and some terrestrial samples. Geochim. Cosmochim. Acta 222, 17–33.
- Fischer-Gödde, M., Elfers, B.-M., Münker, C., Szilas, K., Maier, W.D., Messling, N., Morishita, T., Van Kranendonk, M., Smithies, H., 2020. Ruthenium isotope vestige of Earth's pre-late-veneer mantle preserved in Archaean rocks. Nature 579, 240–244.
- Fischer-Gödde, M., Kleine, T., 2017. Ruthenium isotopic evidence for an inner Solar System origin of the late veneer. Nature 541, 525–527.
- Fischer-Gödde, M., Burkhardt, C., Kruijer, T.S., Kleine, T., 2015. Ru isotope heterogeneity in the solar protoplanetary disk. Geochim. Cosmochim. Acta 168, 151–171.
- Fujii, T., Moynier, F., Albarede, F., 2006. Nuclear field vs. nucleosynthetic effects as cause of isotopic anomalies in the early Solar System. Earth Planet. Sci. Lett. 247, 1–9
- Goderis, S., Brandon, A.D., Mayer, B., Humayun, M., 2015. s-process Os isotope enrichment in ureilites by planetary processing. Earth Planet. Sci. Lett. 431, 110, 119
- Greber, N.D., Puchtel, I.S., Nägler, T.F., Mezger, K., 2015. Komatiites constrain molybdenum isotope composition of the Earth's mantle. Earth Planet. Sci. Lett. 421, 129–138

- Hellmann, J.L., Hopp, T., Burkhardt, C., Becker, H., Fischer-Gödde, M., Kleine, T., 2021. Tellurium isotope cosmochemistry: Implications for volatile fractionation in chondrite parent bodies and origin of the late veneer. Geochim. Cosmochim. Acta 309, 313–328.
- Hilton, C.D., Bermingham, K.R., Walker, R.J., McCoy, T.J., 2019. Genetics, crystallization sequence, and age of the South Byron Trio iron meteorites: New insights to carbonaceous chondrite (CC) type parent bodies. Geochim. Cosmochim. Acta 251, 217–228.
- Hilton, C.D., Walker, R.J., 2020. New implications for the origin of the IAB main group iron meteorites and the isotopic evolution of the noncarbonaceous (NC) reservoir. Earth Planet. Sci. Lett. 540, 116248.
- Hopp, T., Budde, G., Kleine, T., 2020. Heterogeneous accretion of Earth inferred from Mo-Ru isotope systematics. Earth Planet. Sci. Lett. 534, 116065.
- Izidoro, A., Dasgupta, R., Raymond, S.N., Deienno, R., Bitsch, B., Isella, A., 2021. Planetesimal rings as the cause of the Solar System's planetary architecture. Nat. Astron 6, 357–366.
- Jennings, E.S., Jacobson, S.A., Rubie, D.C., Nakajima, Y., Vogel, A.K., Rose-Weston, L.A., Frost, D.J., 2021. Metal–silicate partitioning of W and Mo and the role of carbon in controlling their abundances in the bulk silicate earth. Geochim. Cosmochim. Acta 293, 40–69.
- Kimura, K., Lewis, R.S., Anders, E., 1974. Distribution of gold and rhenium between nickel-iron and silicate melts: implications for the abundance of siderophile elements on the Earth and Moon. Geochim. Cosmochim. Acta 38, 683–701.
- Kokubo, E., Ida, S., 1998. Oligarchic Growth of Protoplanets. Icarus 131, 171-178.
- Kruijer, T.S., Burkhardt, C., Budde, G., Kleine, T., 2017. Age of Jupiter inferred from the distinct genetics and formation times of meteorites. Proc. Natl. Acad. Sci. 114, 6712–6716.
- Kruijer, T.S., Burkhardt, C., Borg, L.E., Kleine, T., 2022. Tungsten and molybdenum isotopic evidence for an impact origin of pallasites. Earth Planet. Sci. Lett. 584, 117440.
- Liang, Y.-H., Halliday, A.N., Siebert, C., Fitton, J.G., Burton, K.W., Wang, K.-L., Harvey, J., 2017. Molybdenum isotope fractionation in the mantle. Geochim. Cosmochim. Acta 199, 91–111.
- Lichtenberg, T., Drążkowska, Joanna, Schönbächler, Maria, Golabek Gregor, J., Hands Thomas, O., 2021. Bifurcation of planetary building blocks during Solar System formation. Science 371, 365–370.
- Liu, N., Stephan, T., Boehnke, P., Nittler, L.R., Alexander, C.M.O., Wang, J., Davis, A.M., Trappitsch, R., Pellin, M.J., 2017. J-type carbon stars: a dominant source of ¹⁴N-rich presolar SiG grains of type AB. The Astrophysical Journal Letters 844, L12–L119.
- Ludwig K.R., 1991. ISOPLOT; a plotting and regression program for radiogenic-isotope data; version 2.53.
- Marchi, S., Canup, R.M., Walker, R.J., 2018. Heterogeneous delivery of silicate and metal to the Earth by large planetesimals. Nat. Geosci. 11, 77–81.
- Marti, K., Fischer-Gödde, M., Proksche, C., 2023. Meteoritic molybdenum and ruthenium isotopic abundances document nucleosynthetic p-process components. Astrophys J 956, 7–13.
- Meisel, T., Walker, R.J., Irving, A.J., Lorand, J.-P., 2001. Osmium isotopic compositions of mantle xenoliths: a global perspective. Geochim. Cosmochim. Acta 65, 1311-1323
- Mundl-Petermeier, A., Walker, R.J., Fischer, R.A., Lekic, V., Jackson, M.G., Kurz, M.D., 2020. Anomalous ¹⁸²W in high ³He/⁴He ocean island basalts: Fingerprints of Earth's core? Geochim. Cosmochim. Acta 271, 194–211.
- Nagai, Y., Yokoyama, T., 2016. Molybdenum isotopic analysis by negative thermal ionization mass spectrometry (N-TIMS): effects on oxygen isotopic composition. J. Anal. At. Spectrom 31, 948–960.
- Nakanishi, N., Yokoyama, T., Ishikawa, A., Walker, R.J., Abe, Y., Aléon, J., O'D Alexander, C.M., Amari, S., Amelin, Y., Bajo, K.-I., Bizzarro, M., Bouvier, A., Carlson, R.W., Chaussidon, M., Choi, B.-G., Dauphas, N., Davis, A.M., Di Rocco, T., Fujiya, W., Fukai, R., Gautam, I., Haba, M.K., Hibiya, Y., Hidaka, H., Homma, H., Hoppe, P., Huss, G.R., Ichida, K., Iizuka, T., Ireland, T.R., Itoh, S., Kawasaki, N., Kita, N.T., Kitajima, K., Kleine, T., Komatani, S., Krot, A.N., Liu, M.-C., Masuda, Y., Morita, M., Motomura, K., Moynier, F., Nakai, I., Nagashima, K., Nguyen, A., Nittler, L., Onose, M., Pack, A., Park, C., Piani, L., Qin, L., Russell, S.S., Sakamoto, N., Schönbächler, M., Tafla, L., Tang, H., Terada, K., Terada, Y., Usui, T., Wada, S., Wadhwa, M., Yamashita, K., Yin, Q.-Z., Yoneda, S., Young, E.D., Yui, H., Zhang, A. C., Nakamura, T., Naraoka, H., Noguchi, T., Okazaki, R., Sakamoto, K., Yabuta, H., Abe, M., Miyazaki, A., Nakato, A., Nishimura, M., Okada, T., Yada, T., Yogata, K., Nakazawa, S., Saiki, T., Tanaka, S., Terui, F., Tsuda, Y., Watanabe, S.-I., Yoshikawa, M., Tachibana, S., Yurimoto, H., 2023. Nucleosynthetic s-process depletion in Mo from Ryugu samples returned by Hayabusa2. Geochem. Perspect. Lett. 28, 31-36.
- Nicolussi, C.K., Pellin, M.J., Lewis, R.S., Davis, A.M., Amari, S., Clayton, R.N., 1998. Molybdenum isotopic composition of individual presolar silicon carbide grains from the murchison meteorite. Geochim. Cosmochim. Acta 62, 1093–1104.
- Poole, G.M., Rehkämper, M., Coles, B.J., Goldberg, T., Smith, C.L., 2017. Nucleosynthetic molybdenum isotope anomalies in iron meteorites – new evidence for thermal processing of solar nebula material. Earth Planet. Sci. Lett. 473, 215–226.
- Rizo, H., Walker, R.J., Carlson, R.W., Touboul, M., Horan, M.F., Puchtel, I.S., Boyet, M., Rosing, M.T., 2016. Early Earth differentiation investigated through ¹⁴²Nd, ¹⁸²W, and highly siderophile element abundances in samples from Isua, Greenland. Geochim. Cosmochim. Acta 175, 319–336.

- Rizo, H., Andrault, D., Bennett, N.R., Humayun, M., Brandon, A., Vlastelic, I., Moine, B., Poirier, A., Bouhifd, M.A., Murphy, D.T., 2019. ¹⁸²W evidence for core-mantle interaction in the source of mantle plumes. Geochem. Perspect. Lett. 6–11.
- Rudge, J.F., Reynolds, B.C., Bourdon, B., 2009. The double spike toolbox. Chem. Geol. 265, 420-431.
- Siebert, C., Nägler, T.F., Kramers, J.D., 2001. Determination of molybdenum isotope fractionation by double-spike multicollector inductively coupled plasma mass spectrometry. Geochem. Geophys. Geosyst. 2, 2000GC000124.
- Spitzer, F., Burkhardt, C., Budde, G., Kruijer, T.S., Morbidelli, A., Kleine, T., 2020. Isotopic evolution of the inner solar system inferred from molybdenum isotopes in meteorites. Astrophys J 898, L2–L12.
- Spitzer, F., Burkhardt, C., Pape, J., Kleine, T., 2021. Collisional mixing between inner and outer solar system planetesimals inferred from the Nedagolla iron meteorite. Meteorit. Planet. Sci. 57, 261–276.
- Stephan, T., Davis, A.M., 2021. Molybdenum isotope dichotomy in meteorites caused by s-process variability. Astrophys J 909, 8–29.
- Stephan, T., Trappitsch, R., Hoppe, P., Davis, A.M., Pellin, M.J., Pardo, O.S., 2019. Molybdenum Isotopes in Presolar Silicon Carbide Grains: Details of s-process Nucleosynthesis in Parent Stars and Implications for r- and p-processes. Astrophys J 877. 101–117.
- Tornabene, H.A., Hilton, C.D., Bermingham, K.R., Ash, R.D., Walker, R.J., 2020. Genetics, age and crystallization history of group IIC iron meteorites. Geochim. Cosmochim. Acta 288, 36–50.
- Tornabene, H.A., Ash, R.D., Walker, R.J., Bermingham, K.R., 2023. Genetics, age, and crystallization history of group IC iron meteorites. Geochim. Cosmochim. Acta 340, 108–119
- Trinquier, A., Birck, J., Allegre, C.J., 2007. Widespread ⁵⁴Cr heterogeneity in the inner solar system. Astrophys J 655, 1179–1185.
- Varas-Reus, M.I., König, S., Yierpan, A., Lorand, J.-P., Schoenberg, R., 2019. Selenium isotopes as tracers of a late volatile contribution to Earth from the outer Solar System. Nat. Geosci. 12, 779–782.
- Walker, R.J., 2009. Highly siderophile elements in the Earth, Moon and Mars: Update and implications for planetary accretion and differentiation. Geochemistry 69, 101–125
- Wang, Z., Becker, H., 2013. Ratios of S, Se and Te in the silicate Earth require a volatilerich late veneer. Nature 499, 328–331.
- Warren, P.H., 2011. Stable-isotopic anomalies and the accretionary assemblage of the Earth and Mars: A subordinate role for carbonaceous chondrites. Earth Planet. Sci. Lett. 311, 93–100.
- Weis, D., Kieffer, B., Maerschalk, C., Barling, J., de Jong, J., Williams, G.A., Hanano, D., Pretorius, W., Mattielli, N., Scoates, J.S., Goolaerts, A., Friedman, R.M., Mahoney, J. B., 2006. High-precision isotopic characterization of USGS reference materials by TIMS and MC-ICP-MS. Geochem. Geophys. Geosyst. 7, Q08006.
- Worsham, E.A., Bermingham, K.R., Walker, R.J., 2017. Characterizing cosmochemical materials with genetic affinities to the Earth: Genetic and chronological diversity within the IAB iron meteorite complex. Earth Planet. Sci. Lett. 467, 157–166.
- Worsham, E.A., Burkhardt, C., Budde, G., Fischer-Gödde, M., Kruijer, T.S., Kleine, T., 2019. Distinct evolution of the carbonaceous and non-carbonaceous reservoirs: Insights from Ru. Mo. and W. isotones. Earth Planet. Sci. Lett. 521, 103–112.
- Insights from Ru, Mo, and W isotopes. Earth Planet. Sci. Lett. 521, 103–112. Worsham, E.A., Kleine, T., 2021. Late accretionary history of Earth and Moon preserved in lunar impactites. Sci. Adv. 7, eabh2837.
- Worsham, E.A., Walker, R.J., Bermingham, K.R., 2016. High-precision molybdenum isotope analysis by negative thermal ionization mass spectrometry. Int. J. Mass Spectrom. 407, 51–61.
- Yobregat, E., Fitoussi, C., Pili, E., Touboul, M., 2022. High-precision measurements of Mo isotopes by N-TIMS. Int. J. Mass Spectrom. 476, 116846.
- Yokoyama, T., Alexander, C.M.O., Walker, R.J., 2011. Assessment of nebular versus parent body processes on presolar components present in chondrites: Evidence from osmium isotopes. Earth Planet. Sci. Lett. 305, 115–123.
- Yokoyama, T., Nagai, Y., Fukai, R., Hirata, T., 2019. Origin and evolution of distinct molybdenum isotopic variabilities within carbonaceous and noncarbonaceous reservoirs. Astrophys J 883, 62–85.
- Yokoyama, T., Ohkuma, Y., Nishikawa, K., Sumiya, K., Gautam, I., 2023a. Evaluation of the residual mass fractionation in high-precision Cr isotopic analysis with TIMS. Geostand. Geoanal. Res. 47, 415–435.
- Yokoyama, T., Wadhwa, M., Iizuka, T., Rai, V., Gautam, I., Hibiya, Y., Masuda, Y., Haba, M.K., Fukai, R., Hines, R., Phelan, N., Abe, Y., Aléon, J., Alexander, C.M.O., Amari, S., Amelin, Y., Bajo, K., Bizzarro, M., Bouvier, A., Carlson, R.W., Chaussidon, M., Choi, B.-G., Dauphas, N., Davis, A.M., Di Rocco, T., Fujiya, W., Hidaka, H., Homma, H., Hoppe, P., Huss, G.R., Ichida, K., Ireland, T., Ishikawa, A., Itoh, S., Kawasaki, N., Kita, N.T., Kitajima, K., Kleine, T., Komatani, S., Krot, A.N., Liu, M.-C., McKeegan, K.D., Morita, M., Motomura, K., Moynier, F., Nakai, I. Nagashima, K., Nguyen, A., Nittler, L., Onose, M., Pack, A., Park, C., Piani, L., Qin, L., Russell, S., Sakamoto, N., Schönbächler, M., Tafla, L., Tang, H., Terada, K. Terada, Y., Usui, T., Wada, S., Walker, R.J., Yamashita, K., Yin, Q.-Z., Yoneda, S., Young, E.D., Yui, H., Zhang, A.-C., Nakamura, T., Naraoka, H., Noguchi, T., Okazaki, R., Sakamoto, K., Yabuta, H., Abe, M., Miyazaki, A., Nakato, A., Nishimura, M., Okada, T., Yada, T., Yogata, K., Nakazawa, S., Saiki, T., Tanaka, S., Terui, F., Tsuda, Y., Watanabe, S., Yoshikawa, M., Tachibana, S., Yurimoto, H., 2023b. Water circulation in Ryugu asteroid affected the distribution of nucleosynthetic isotope anomalies in returned sample. Sci. Adv. 9, eadi7048.